Preprints (www.preprints.org) | NOT PEER-REVIEWED | Posted: 19 April 2023 doi:10.20944/preprints202304.0595.v1

Disclaimer/Publisher's Note: The statements, opinions, and data contained in all publications are solely those of the individual author(s) and contributor(s) and not of MDPI and/or the editor(s). MDPI and/or the editor(s) disclaim responsibility for any injury to people or property resulting from any ideas, methods, instructions, or products referred to in the content.

Article

Polyvinylpyrrolidone nanofibers incorporating mesoporous bioactive glass for bone tissue engineering

Ricardo J. R. Matos [1], Jorge C. Silva [2,*], Paula I. P. Soares [1,*] and João Paulo Borges [1]

[1] i3N/CENIMAT, Department of Materials Science, NOVA School of Science and Technology, NOVA University Lisbon, Campus de Caparica, Caparica, Portugal;
[2] i3N/CENIMAT, Department of Physics, NOVA School of Science and Technology, NOVA University Lisbon, Campus de Caparica, Caparica, Portugal;
* Correspondence: jcs@fct.unl.pt and pi.soares@fct.unl.pt

Abstract: Composite biomaterials that combine osteoconductive and osteoinductive properties are a promising approach for bone tissue engineering (BTE) since it allows osteogenesis stimulation while mimicking the extracellular matrix (ECM) morphology. In this context, the aim of the present research work was to produce polyvinylpyrrolidone (PVP) nanofibers containing mesoporous bioactive glass (MBG) 80S15 nanoparticles. These composite materials were produced by electrospinning technique. The design of experiments (DOE) was used to estimate the optimal electrospinning parameters to reduce average fiber diameter. The polymeric matrices were thermally crosslinked under different conditions, and the fiber's morphology was studied using scanning electron microscopy (SEM). Evaluation of the mechanical properties of nanofibrous mats revealed a dependence on thermal crosslinking parameters and on the presence of MBG 80S15 particles inside the polymeric fibers. Degradation tests indicated that the presence of MBG led to a faster degradation of nanofibrous mats. On the other hand, MBG presence also leads to higher swelling capacity. The assessment of in vitro bioactivity in simulated body fluid (SBF) was performed in MBG pellets and PVP/MBG (1:1) composites to assess whether the bioactive properties of MBG 80S15 were kept when it was incorporated into PVP nanofibers. FTIR and XRD analysis along with SEM–EDS results indicated that a hydroxy-carbonate apatite (HCA) layer was formed on the surface of MBG pellets and nanofibrous webs after soaking in SBF over different time periods. In general, the materials revealed no cytotoxic effects on Saos-2 cell line. The overall results for the produced materials show the potential of the composites to be used in BTE.

Keywords: Electrospun polyvinylpyrrolidone; polymeric scaffolds; bone regeneration; mesoporous bioactive glass.

1. Introduction

Bone is one of the most transplanted tissues, second only to blood [1]. Generally, large bone defects mainly result from fractures or diseases, such as bone cancer, and often became unable to heal spontaneously by the natural body's repair mechanisms. Bone tissue engineering (BTE) has gained more relevance over the last few years since it can offer promising approaches to bone defects treatment by providing the stimulus and osteoconductive templates to guide the regeneration of new bone tissue [2]. Moreover, biomaterials used for BTE should be also angiogenic, as they should induce the formation of blood vessels in the constructs to ensure the newly regenerated tissue receives the proper quantity of oxygen and nutrients to ensure its survival [3].

Bioactive glasses (BGs) are mostly applied in BTE since it allows to fabricate optimal scaffolds with osteogenic and angiogenic potential [4]. 45S5 Bioglass® particles have demonstrated interesting results on potential angiogenic effects, considering the increased secretion of vascular endothelial growth factor (VEGF) *in vitro* and enhancement of

© 2023 by the author(s). Distributed under a Creative Commons CC BY license.

Preprints (www.preprints.org) | NOT PEER-REVIEWED | Posted: 19 April 2023 doi:10.20944/preprints202304.0595.v1

vascularization *in vivo* [5]. In addition, it has been demonstrated by Hench and Polak that dissolution products from BGs induce a genetic control over the osteoblast cell cycle and the rapid expression of genes that regulate osteogenesis [6]. All bioactive glasses, being melt or sol–gel derived, can induce bioreactivity or bioactivity due to the ability to interact with living tissue forming strong bonds to bone. These strong bonds are formed by the precipitation of a hydroxy-carbonate apatite (HCA) layer on the BG surface when in contact with relevant physiological fluid or during *in vivo* applications [7].

Since the discovery of Bioglass by Hench *et al.* in the early I970s [8], various kinds of glasses and glass-ceramics have been found to bond to living bone. Recently, a new family of mesoporous bioactive glasses (MBGs) with highly ordered mesoporous structures and larger specific surface area showed promising features for BTE. The increased interface effects lead to high reactivity, thus improving the bioactivity when compared to standard BGs. Mesoporous materials are mainly dependent on the use of surfactants as structure-directing agents for the inorganic component to form channels, thus creating highly ordered mesoporous when the surfactant is removed [9].

BGs and MBGs can be produced to feature different morphologies (e.g., powder, granules, monoliths, fiber, or coatings, etc.) [10]. Both micron-sized and nanoscale powder particles should be considered in this application field, which can be used in the production of composite material scaffolds, such as the combination of electrospun biodegradable polymers and MBGs, which is the purpose of this work. The main advantage of these composite materials is to maintain the bioactivity of the inorganic bioactive filler while keeping the mechanical properties of the polymer (e.g., flexibility and capacity to deform under loads). Moreover, the use of MBG nanoparticles in a polymeric matrix mimic more closely the structure of natural bone, which contains nanoscale hydroxyapatite crystallites combined with the polymeric phase of collagen type I, being responsible for the desirable mechanical properties of bone [7]. From this point of view, the size of the BGs or MBGs particles incorporated in the polymeric matrices also plays an important role in enhancing bioactivity. There is evidence in literature that mimicking the nanofeatures of bone increase bone-forming cell adhesion and proliferation [11].

Polyvinylpyrrolidone (PVP) is a synthetic polymer with high solubility in water as well as many organic solvents. PVP has been widely used in the development of hydrogels, wound dressings, nanofibers/scaffolds, drug, and gene delivery systems, and most famously as a blood plasma substitute during World War II. It is used in tissue engineering/repair as well [12].

In this paper, we have successfully prepared a mesoporous bioactive glass MBG 80S15, by using Pluronic F127 as a structure-directing agent through an evaporation-induced self-assembly (EISA) process. MBG 80S15 nanosized powder was further incorporated into PVP electrospun nanofibers, and its properties were studied to assess the potential of such composites to be used in BTE applications. Furthermore, the coupling of PVP with MBG nanoparticles produces composite 2D materials where it is possible to control the degradation and bioactivity rates to fit the natural processes of bone repair.

2. Materials and Methods

All the chemical reagents used in this research work were of analytical grade and used without further purification.

2.1. Synthesis of Mesoporous Bioactive Glass MBG 80S15

Mesoporous Bioactive Glass MBG 80S15 is a ternary bioactive glass SiO_2–CaO–P_2O_5, which was produced by a sol-gel technique adapted from a previously described method by Yan *et al.*, [13]. MBG was synthesized by using nonionic block copolymer – *Pluronic* F127 ($EO_{106}PO_{70}EO_{106}$) (*Sigma-Aldrich*) as structure-directing agents (EO is poly(ethylene oxide), and PO is poly(propylene oxide)). In a typical synthesis of MBG 80S15, in order to achieve a molar ratio of Si/Ca/P=80:15:5, tetraethyl orthosilicate (*Sigma-Aldrich*) (TEOS,

Preprints (www.preprints.org) | NOT PEER-REVIEWED | Posted: 19 April 2023 doi:10.20944/preprints202304.0595.v1

6.7 g), calcium nitrate-4-hydrate (*PanReac AppliChem*) $Ca(NO_3)_2{\cdot}4H_2O$ (1.4 g), triethyl phosphate (*Sigma-Aldrich*) (TEP, 0.73 g), and 0.5 *M* HCl (1.0 g) were dissolved in absolute ethanol (*Sigma-Aldrich*) (60 g). TEOS, TEP and calcium nitrate-4-hydrate were used as precursors of SiO_2, P_2O_5 and CaO, respectively. The mixture was allowed to react for 30 min for the acid hydrolysis of TEOS. Then, 1.82 g of *Pluronic* F127 was added to the mixture and the resultant solution was stirred at room temperature for 60 hours to undergo an evaporation-induced self-assembly (EISA) process. The obtained gel was heated at 60 °C for 24 hours to completely remove the alcohol. Subsequently, the dried gel was calcined at 700 °C for 5 hours (ramp of 2 °C.min^{-1}) to obtain the final MBG 80S15 products. The resulting powder was grounded in a planetary ball-milling (Planetary Mono Mill Pulverisette 6) for 6 hours using zirconia balls. The final average grain size was about 150 ± 72 nm.

2.2. Optimization of electrospinning process by DOE

An 18 w/v % PVP ($M_w \sim 1\,300\,000\ g/mol$) (*Sigma-Aldrich*) solution in ethanol (*Sigma-Aldrich*) was prepared and used for electrospinning. Electrospinning was performed at 20°C with humidity around 40%. In this study, the environmental conditions and the solution parameters were kept constant. Four operating variables (flow rate, tip-collector distance, applied voltage, and needle's gauge) were studied by applying a Custom Design of Experiments and the response surface methodology (RSM) as a statistical method. The custom DOE was performed using *JMP software version 13.0* (S.A.S. Institute Inc., Cary, NC, USA) to investigate the effect of above-mentioned electrospinning process parameters and the interactions between these variables on the electrospun PVP average fiber diameter.

The range of each variable was chosen considering the set of values that allow the PVP electrospinning process based on literature and previous experiences (Table 1). Within the range defined for each variable, the software selected a set of experiments consisting of a minimum of 27 runs. To determine how to optimize the parameters, several outputs were measured: the samples were analyzed by SEM to observe the overall structure of the collected mats and the average fiber diameter was calculated using *ImageJ Software* by selecting at least 25 random fibers. Using the RSM, the overall desirable response (set of variables that minimizes the average fiber diameter) was obtained from the software's calculations within the pre-selected range of each variable. The software also estimated the resulting PVP average fiber diameter for that set of variables, which was about 652 ± 179 nm.

In addition, for all the experiments and subsequent membrane production, the polymer solution was placed in a 1 mL syringe, and dispensed by a syringe pump (*KDS100, KD Scientific)* at different rates from 0.1 to 0.4 mL.h^{-1}. A high voltage supply (*Glassman EL 30kV*) was connected to the metallic needle (ITEC), and a sheet of aluminum foil was used as collector and placed in front of the needle tip at distances ranging from 15 to 20 cm to collect the fibers.

Table 1. Range of four independent variables of a custom design of experiments (JMP software) aiming to minimize the electrospun PVP average fiber diameter, and respective desirable response using RSM.

Variable	Type	Range	Desirable response	Estimated Output (nm)
Applied voltage (kV)	Continuous	15-20	18.6	652 ± 179
Flow rate (mL.h-1)	Continuous	0.1-0.4	0.1	
Tip-collector distance (cm)	Continuous	15-20	17.3	
Needle's gauge	Categorical	G23; G27	G27	

2.2.1. PVP/MBG composite production

Preprints (www.preprints.org) | NOT PEER-REVIEWED | Posted: 19 April 2023 doi:10.20944/preprints202304.0595.v1

To obtain the solution for electrospinning, the MBG powder was first added to ethanol and subsequently sonicated for 15 min at 320 W for further dispersion. PVP was weighed and dissolved in the previously dispersed solution containing the solvent to obtain a final polymer concentration of 18 w/v %. The final blend was magnetically stirred for at least 30 min resulting in a well-dispersed MBG powder into the polymeric solution. Different percentages of the MBG powder were added to ethanol for further dispersion: 10; 28; 56; 83; and 100 % by weight with respect to PVP content. It is important to mention that the amount of bioactive glass particles used in this work should be significant to induce bioactivity and simultaneously tailor the degradation rate of PVP. In this context, the composites containing 100 % MBG by weight with respect to PVP are of major interest. From now on, this composite will be denominated PVP/MBG (1:1) as the mass content of MBG and PVP is the same.

Electrospinning was carried out with the same processing parameters estimated from the DOE to plain PVP, except the needle's gauge. The composites were electrospun with a G23 needle (ITEC) to prevent clogging. The produced membranes were kept in a desiccator until the crosslinking treatment due to the water solubility of PVP.

2.2.2. Thermal Crosslinking

PVP is water soluble, which limits the applicability of electrospun PVP-based nanofibers if left without any treatment. However, PVP is known to decrease in solubility upon heating in air between 150 and 200 °C [14]. The as-spun PVP and PVP/MBG composites were crosslinked in an incubator (Memmert Incubator Modell 100-800) at different temperatures within the above-mentioned range. Final temperatures of 150, 165, and 180 °C were studied for different times: 3, 4, 5, 8, 12, and 24 h. To investigate the effect of thermal crosslinking, the membranes were immersed for 24 hours in the water, dried at 60 °C and analyzed by SEM.

2.3. Characterization

Transmission electron microscopy (TEM) images were obtained using a Hitachi H-8100II with thermo-ionic emission LaB_6 with a resolution of 2.7 Å. The membranes' analysis was performed on the thinnest membrane that can be technically extracted (around 15-20 min deposition).

The crystalline phases of the samples were verified using powder X-ray diffraction (XRD). X'Pert PRO PANAlytical X-ray diffractometer was used to obtain X-ray diffraction patterns. The 2θ values were taken from 15° to 80° using a Cu-Kα radiation (λ = 1.54060 Å) with a step size of 0.033.

FTIR spectra of the samples were obtained using a Nicolet 6700–Thermo Electron Corporation Attenuated Total Reflectance- Fourier Transform Infrared spectrometer (ATR-FTIR). Measurements were performed in the range of 480–4000 cm^{-1} with a resolution of 2 cm^{-1}.

Scanning electron microscopy (SEM) that allowed fiber morphology analysis was performed using a Carl Zeiss Auriga SEM equipment. The samples were coated with a thin layer of iridium-palladium or carbon depending on which elements were being studied by EDS analysis.

N_2 adsorption–desorption isotherms were measured with a Gas Porosimeter Micromeritics ASAP 2010 at -196 °C. Before the measurements, the samples were outgassed at 300 °C in vacuum for 12 hours. The Barrett–Emmett–Teller (BET) method was utilized to calculate the specific surface area. The pore volume and pore-size distribution were derived from the adsorption branches of the isotherms using the Barrett–Joyner–Halanda (BJH) method. The total pore volume was estimated from the adsorbed amount at a maximum relative pressure.

Thermo-gravimetric analysis (TGA) curves were recorded with the Simultaneous Thermal Analyser STA 449 F3 Jupiter under an inert nitrogen atmosphere at a heating rate

Preprints (www.preprints.org) | NOT PEER-REVIEWED | Posted: 19 April 2023 doi:10.20944/preprints202304.0595.v1

of 10 °C/min from room temperature to 900 °C. Differential TGA (DTGA) was obtained by differentiating the respective TGA curve.

2.4. Swelling and Degradation assays

The success of thermal crosslinking was studied by testing the dissolution of cross-linked mats immersed in phosphate buffer solution (PBS, pH 7.4) at 37 °C for different time points: 1, 3, 7, 13, 17, 21, and 28 days. At these time points the degradation of PVP and PVP/MBG composites fibers in physiological solutions was assessed by measuring the membranes' weight loss. The samples were removed from PBS, gently rinsed with Millipore water to remove saline, and dried at 37 °C until constant mass was reached The percentage of weight loss (W_L %) was computed as $W_L\,\% = 100 \times \frac{(W_0 - W_r)}{W_0}$, where W_0 and W_r are the initial and the residual weight of the sample, respectively.

The swelling ratio is a measure of the liquid absorbing capacity of a matrix. The dry weight of each sample was measured (W_d) before soaking into PBS (pH 7.4). The mass of each sample was planned to be at least 10 mg ensuring the membrane stability over the experiment. At pre-determined intervals of time (5, 15, and 30 min; 1 and 5 h; 1, 3, and 7 days) the specimens were removed from the PBS. The excess liquid on each matrix was removed, and the wet matrices were weighed (W_w). The swelling ratio (Q) was calculated as: $Q = \frac{W_w - W_d}{Wd}$

In both degradation and swelling experiments, all samples were cut with dimensions of 20 mm x 20 mm and placed in a plastic container (Falcon tube, 50 mL) filled with PBS (pH 7.4). The experiments were performed in an incubator with an orbital shaker (Comecta - Heated Incubator with Shaker S-100D) at 37 °C. An average of at least three samples was taken for each time point. The samples were weighed with an accuracy of 0.1 mg on an analytical balance (Sartorious Quintix Model 224-1S).

2.5. Mechanical response – tensile tests

The tensile tests were performed on a Rheometric Scientific uniaxial tensile testing machine with 20 N load cell and operable through the Minimat software (Minimat Control Software Version 1.60 February 1994 (c) PL Thermal Science 1984-94 Reometric Scientific Ltd.). A velocity of 1 mm.min^{-1} was applied in all experiments, which were performed at room temperature and humidity around 50%. For each type of membrane at least 10 samples were measured. The samples were cut into a rectangular shape of 10 mm wide and 20 mm long. The thickness of the samples was measured with a digital micrometer (Mitutoyo 0-25 mm). Ultimate tensile strength, Young's modulus and yield strength were determined from stress-strain curves.

2.6. Cytotoxicity assays

To evaluate the cytotoxicity of the membranes, the assays were performed according to standard ISO-10993 Biological evaluation of medical devices, Part 5: Tests for *in vitro* cytotoxicity. The assays were performed using the extract method and Saos-2cell line. To produce the extract, different samples were cut to have an identical mass of 30 mg and pre-sterilized at 120 °C for 2 h. Each sample was placed in 1.5 mL (resulting in an extract concentration of 20 mg.mL^{-1}) of Dulbecco's modified Eagle's medium (DMEM, *Sigma Aldrich*) at 37 °C for 48 h.

Cells were seeded at a density of 30.000 cell.cm^{-2} in 96-well plates and grown in DMEM supplemented with 10% fetal bovine serum, 1% Penicilin-Streptomycin, sodium pyruvate (100 mM, *Life-Technologies*), and GlutaMAX™ Supplement (*Life-Technologies*) followed by incubation at 37 °C in 5% CO_2 during 24 h. The subsequent step was to exchange the medium for the extract to assess whether the cells survive the next 48 h. Five concentrations of the extract were used: 20, 10, 5, 2.5 and 1.25 mg.mL^{-1} (two-fold serial dilution). For each concentration, 4 replicas were performed. After this period, the medium was removed and a resazurin solution containing 90% of complete culture medium, as

Preprints (www.preprints.org) | NOT PEER-REVIEWED | Posted: 19 April 2023 doi:10.20944/preprints202304.0595.v1

described above, and 10% of a 0.2 mg.mL^{-1} resazurin solution in PBS was added to each well. After 2 h incubation, the absorbance was measured at 570 and 600 nm. Negative control cells were incubated with complete medium. Positive control cells were treated with 10% DMSO to cause cell death. Cell viability is expressed as a percentage of the negative control, given by [% cell viability = treated cells/control cells x 100].

2.7. Bioactivity assay

The bioactivity of PVP/MBG composites, related to the surface deposition of hydroxy-carbonate apatite (HCA) layers, was evaluated by immersing the samples in simulated body fluid (SBF) solution. The SBF has a composition and ionic concentration similar to those of human body plasma, and it was prepared by dissolving respective amounts of reagent chemicals (NaCl (*Sigma-Aldrich*), $NaHCO_3$ (*Sigma-Aldrich*), KCl (*Sigma-Aldrich*), $MgCl_2{\cdot}6H_2O$ (*Sigma-Aldrich*), HCl (*Honeywell Fluka*), $CaCl_2$ (*Carl Roth*), Na_2SO_4 (*Sigma-Aldrich*), $K_2HPO_4{\cdot}3H_2O$ (*VWR*), and $(CH_2OH)_3(CNH)_2$ (*Apollo Scientific*) as the buffering agent) into deionized water according to the procedure described by Kokubo *et al.*, [15, 16]. The prepared SBF was buffered at pH 7.4 with tris (hydroxymethyl aminomethane) and 1 M hydrochloric acid at 37 °C. The polymeric matrices were cut into samples of 15 × 15 mm^2 and subsequently immersed in 50 mL SBF in a falcon tube for different time periods (1, 3, 5, and 10 days). This experiment adopted international standards ISO/FDIS 23317 [17]; the volume of the SBF solution (V_{SBF}) should be at least the volume (mL) determined according to the following formula: $V_{SBF} = \frac{S_A}{10}$, where S_A is the surface area of the samples (mm^2) . During the experiment, the samples were kept at 37 °C in an incubator with orbital shaker (54 rpm), and the SBF solution was refreshed every two days. After the respective soaking period, the samples were removed from SBF, rinsed with Millipore water, and dried at room temperature. The bioactivity assay was performed for both the PVP/MBG (1:1) composites and MBG powder. For the latter, it was necessary to produce pellets by dry pressing. Each pellet was produced from an amount of 300 mg of powder in a hardened steel mold with an inner diameter of 13 mm. The powder was pressed uniaxially at a load of 5 ton for 5 min at room temperature.

Formation of bone like apatite layer on the surface of nanocomposite mats was determined by X-ray diffraction (XRD), Fourier transform infrared spectroscopy (FTIR) analysis, and scanning electron microscopy coupled with energy dispersive spectroscopy (SEM–EDS).

3. Results

3.1. Mesoporous Bioactive Glass MBG 80S15

MBG synthesis was performed by sol-gel method using Pluronic F127 as a structure-directing agent. During the synthesis process, the evaporation of organic solvent progressively increases the block copolymer concentration. When the concentration of Pluronic F127 reaches the critical micelle concentration, micellar aggregates form through the self-assembly process of silica-surfactant composite micelles, which organize into liquid-crystalline mesophases. Calcination process allows to remove the organic surfactant template and retain inorganic framework to obtain highly ordered mesostructured bioactive glass materials [9], [18].

Fig. 1A shows the nitrogen adsorption-desorption isotherms of the MBG 80S15 calcined powder. The shape of the isotherms corresponds to type IV, typical of a mesoporous structure. Furthermore, the sample shows the type H1 hysteresis loops in the relative pressure of about 0.40, which features the cylindrical pores, in accordance with the p6mm mesostructure. The BET surface area of the MBG calculated from the linear part of the BET plot reached 232 m^2.g^{-1}. The pore size distribution curves were calculated from the adsorption and desorption branches using the BJH model. The MBG presents a relatively narrow pore size distribution, and the peak pore size was around 5.9 nm and 6.0 nm for adsorption and desorption branches, respectively. This proximity between pore size results can

Preprints (www.preprints.org) | NOT PEER-REVIEWED | Posted: 19 April 2023 doi:10.20944/preprints202304.0595.v1

be an indicator of a perfect cylindrical channel. The pore volume was also calculated using the BJH model and the result was about 0.25 $cm^3.g^{-1}$ for both the adsorption and desorption branches.

TEM image of MBG 80S15 is shown in **Fig. 1B**. It can be observed brighter spot areas, which can be an indicator of the mesoporous structure as expected. However, the cylindrical ordered structure of the mesoporous is not evident. Analysis of sample structure by TEM is hindered by the powder aggregation due to multiple layers formation, which increases the sample opacity. On the other hand, the TEM equipment resolution also limits the proper visualization of the MBG mesoporosity.

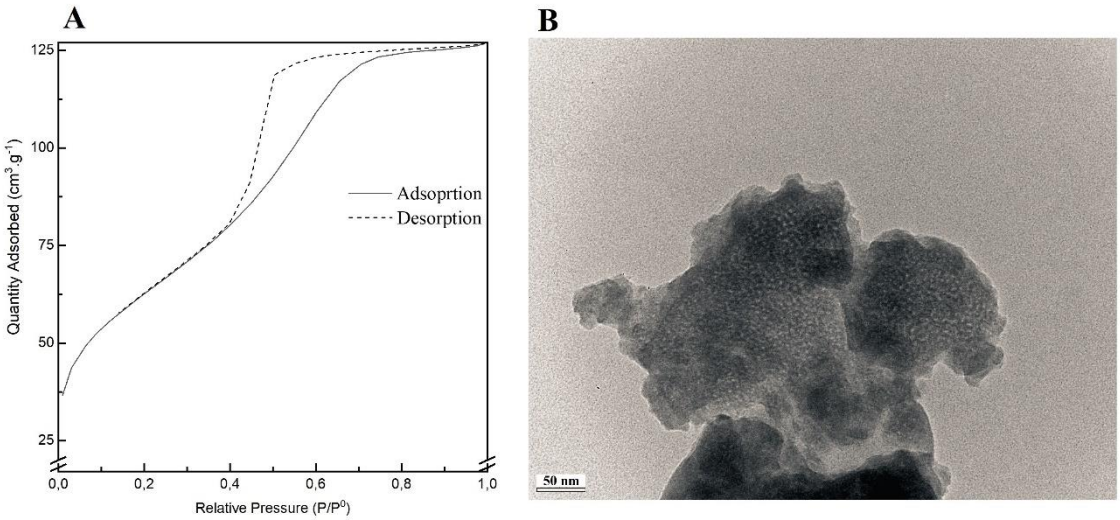

Fig. 1. Nitrogen adsorption-desorption isotherms (A) and TEM image (B) of MBG 80S15 powder.

SEM image of produced MBG 80S15 after 6 h of planetary ball-milling is presented in **Fig. 2A**. It can be observed that the size of MBG particles is in the nanoscale range as shown in the respective particle size distribution graph **Fig. 2B**. The average diameter of MBG particles is around 146 ± 72 nm. It is worth pointing out the reduced dimensions of these particles considering they become easier to disperse in an electrospinning solution compared to micro-sized MBG particles.

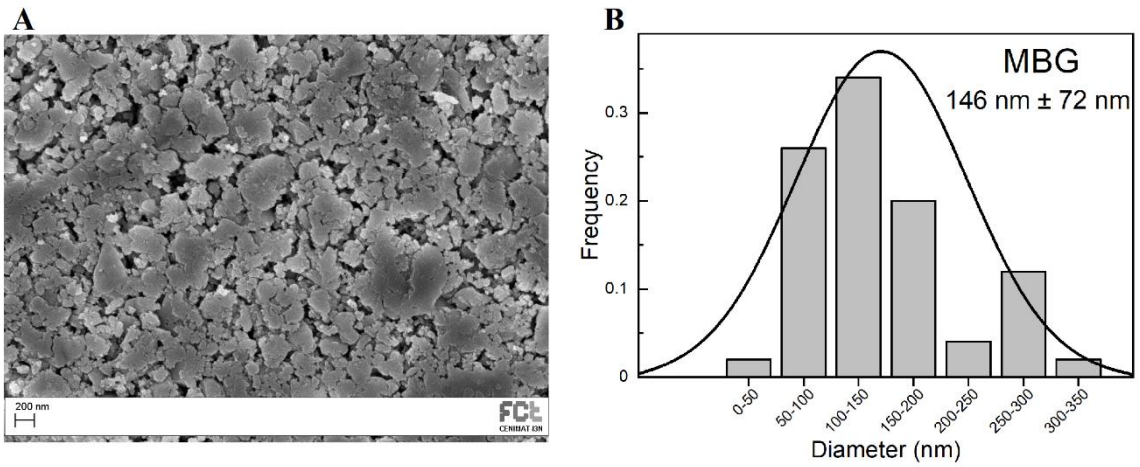

Fig. 2. SEM image of MBG 80S15 pellet (A) and the respective particle size distribution graph after 6 h of ball-milling (B).

Fig. 3 A represents the XRD pattern of the produced MBG 80S15. It can be observed that there are no diffraction peaks appearing on the pattern of the sample, except a broad

Preprints (www.preprints.org) | NOT PEER-REVIEWED | Posted: 19 April 2023 doi:10.20944/preprints202304.0595.v1

reflection at 2θ = 15–35° (characteristic of silicate glasses) which suggests that produced MBG 80S15 exist in amorphous state. The temperature assigned to the occurrence of crystallization is about 810 °C [18]. It is important to note that MBG was calcinated at 700 °C to ensure that mesoporous structure keeps its stability. When the MBGs are calcined at temperatures higher than 810 °C, the inorganic wall becomes crystalline and the mesostructure collapses.

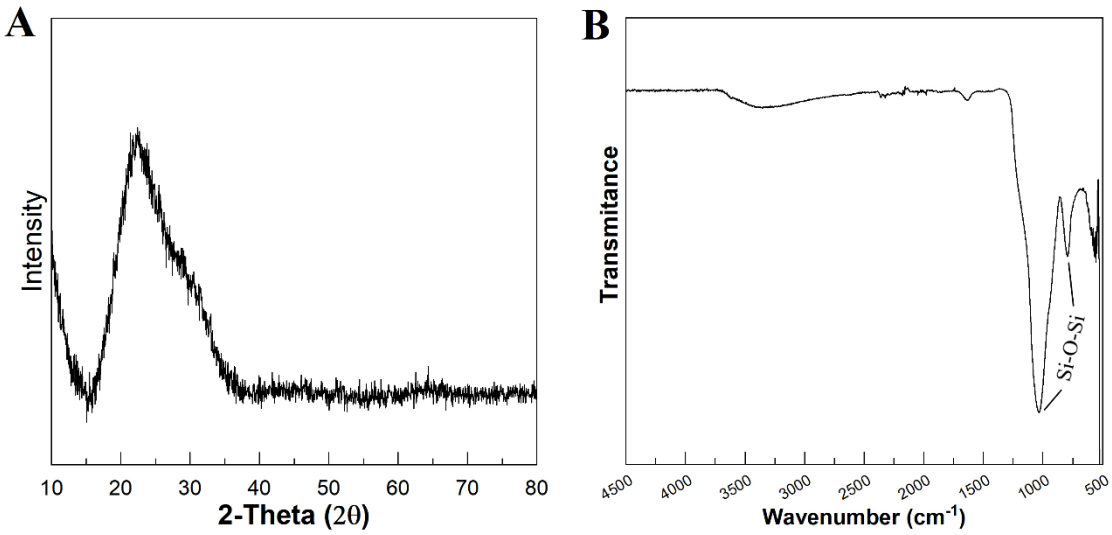

Fig. 3. XRD pattern (A) and FTIR spectra (B) of MBG 80S15 powder calcined at 700 °C for 5 h.

Fig. 3 B shows the FTIR spectrum of the produced MBG 80S15 powder. It is shown that the sample exhibit characteristic absorption bands of a silicate glass. The spectrum shows the Si-O-Si asymmetrical stretching vibration at 1040 cm^{-1} and Si-O-Si symmetrical stretching vibration at 806 cm^{-1}. The band associated to Si-O bending (rocking) vibration at 470 cm^{-1} was not detected due to the equipment resolution (the measuring process starts at 500 cm^{-1}) [19, 20].

3.2. PVP/MBG 80S15 composites

Custom Design of Experiments and RSM as a statistical method allowed to define a set of electrospinning processing parameters that minimize the PVP average fiber diameter as described above (section 2.2). The *JMP software* estimated a resulting PVP average fiber diameter about 652 ± 179 nm for these set of parameters: rate of 0.15 $mL.h^{-1}$; applied voltage of 18.6 kV; tip-collector distance of 17.3 cm; needle's gauge G27 (ITEC). The SEM image and respective average size distribution are shown in **Fig. 4 A** and **B**. SEM micrographs revealed that the electrospun PVP nanofiber mats were composed of randomly oriented, uniform, and bead free nanofibers, with an average diameter size of 656 ± 171 nm, which is quite close to the estimated value from DOE.

Preprints (www.preprints.org) | NOT PEER-REVIEWED | Posted: 19 April 2023 doi:10.20944/preprints202304.0595.v1

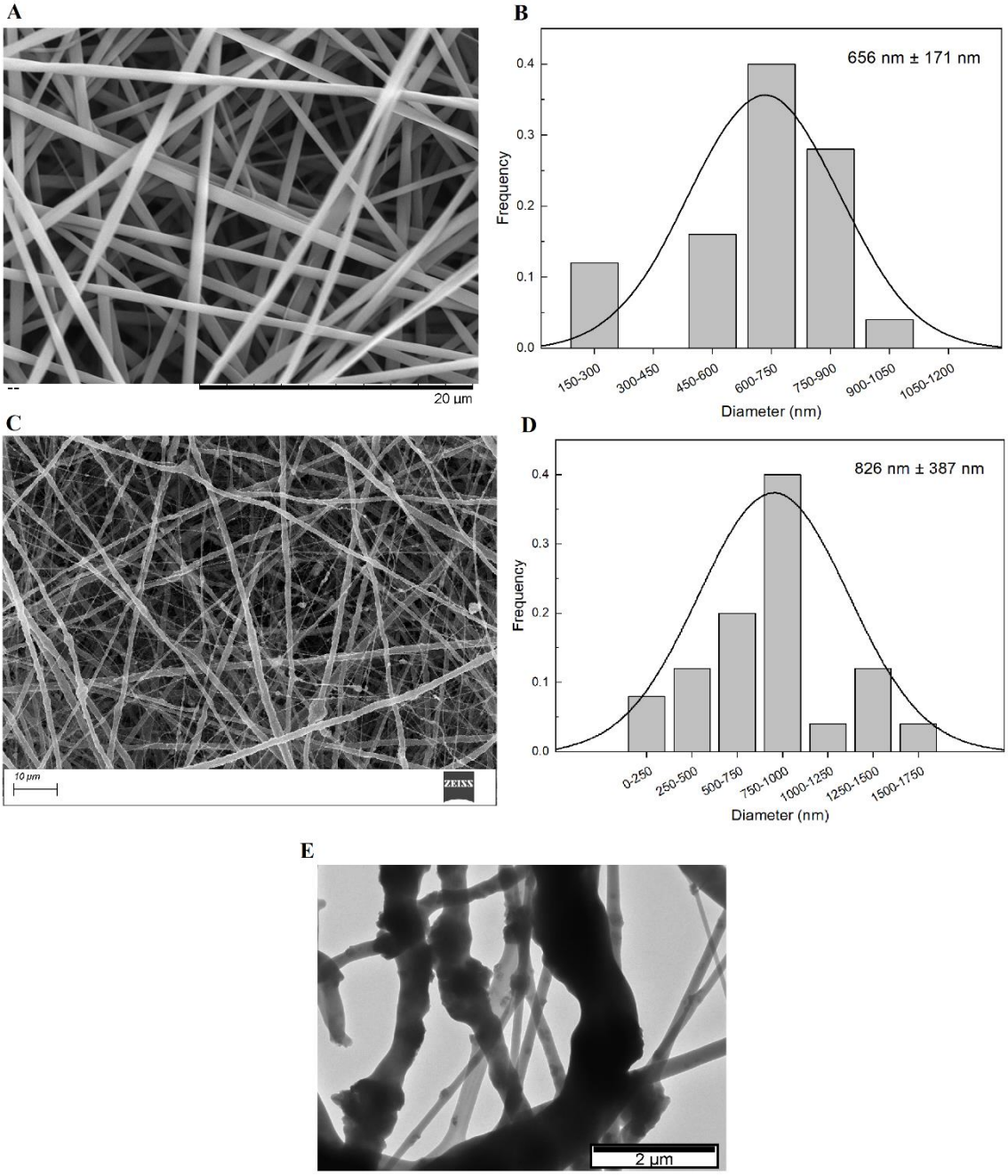

Fig. 4.SEM images and the respective fiber diameter distribution graph of plain PVP membrane (A, B), and PVP/MBG (1:1) composite (C, D). TEM image of PVP/MBG (1:1) composite.

The PVP/MBG composites were electrospun in the same conditions as plain PVP, except the needle's gauge to avoid clogging (G23 ITEC). The SEM image of PVP/MBG (1:1) composite and the respective fiber size distribution is represented in **Fig. 4 C** and **D**. It can be noticed that the incorporation of MBG particles into the PVP fibers changes the fiber's surface. The plain PVP fibers have a smooth surface, which becomes rough and irregular when the MBG particles are incorporated into the fibers, as expected due to the particles' aggregates as shown in TEM image (**Fig. 4 E)**. Consequently, the average fiber diameter and standard deviation of PVP/MBG (1:1) composite fibers increase to 826 nm and 387 nm, respectively. However, composite fibers exhibited a relative homogeneous distribution of embedded MBG 80S15 particles.

Preprints (www.preprints.org) | NOT PEER-REVIEWED | Posted: 19 April 2023 doi:10.20944/preprints202304.0595.v1

TGA analysis was performed on plain PVP, MBG 80S15, and composite electrospun mats PVP/MBG (1:1). The obtained TGA and DTGA curves are reported in **Fig. 5 A** and **B**. All samples show an initial slight mass loss (around 9 %) at 125 °C attributed to the loss of the physical adsorbed water. The thermogram curve for MBG 80S15 previously sintered at 700 °C does not show another considerable mass loss, thus presenting a residual mass of 86.4 % at 900 °C. Meanwhile, the thermogram curve for plain PVP fiber mat showed a steep weight loss between 400 and 480 °C and no considerable residual matter remained after 900 °C indicating complete degradation of the polymer. In the case of PVP/MBG (1:1) nanocomposite fiber mats, 58.6 % weight loss was observed over the temperature range used. This weight loss is associated with water removal and PVP degradation. The residual mass of 41.4 % corroborated the presence of MBG in the nanocomposite mats. The residual mass is consistent with the theoretical amount of MBG content in the composite considering the initial amount introduced in the electrospinning solution. These results along with the SEM and TEM analyses confirmed that composite structures were successfully prepared in the current study.

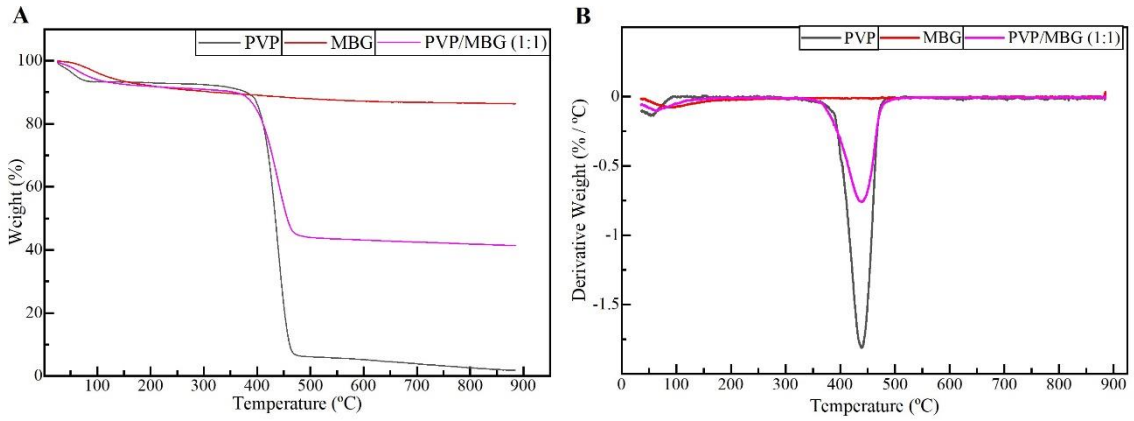

Fig. 5. TGA (A) and DTGA (B) curves of plain PVP (black), PVP/MBG (1:1) composite (purple), and MBG 80S15 calcined at 700 °C (red).

3.3. Swelling and Degradation assays

3.3.1. Thermal crosslinking

PVP is water soluble, thus the as-spun nanofibers need to be crosslinked to make them solvent resistant and suitable for bone tissue engineering (BTE). Thermal treatment was found to be useful as a crosslinker agent of polymer chain segments, as it is easy to apply. Several crosslinking conditions were tested depending on the temperature applied (range: 150 - 200 °C) and time (range: 3 - 24 hours) [14, 21]. However, at temperatures of 165 °C, the membranes showed the most promising results, thus this temperature was kept constant, and different crosslinking times were tested as shown in **Fig. 6** and **Fig. 7**.

Preprints (www.preprints.org) | NOT PEER-REVIEWED | Posted: 19 April 2023 doi:10.20944/preprints202304.0595.v1

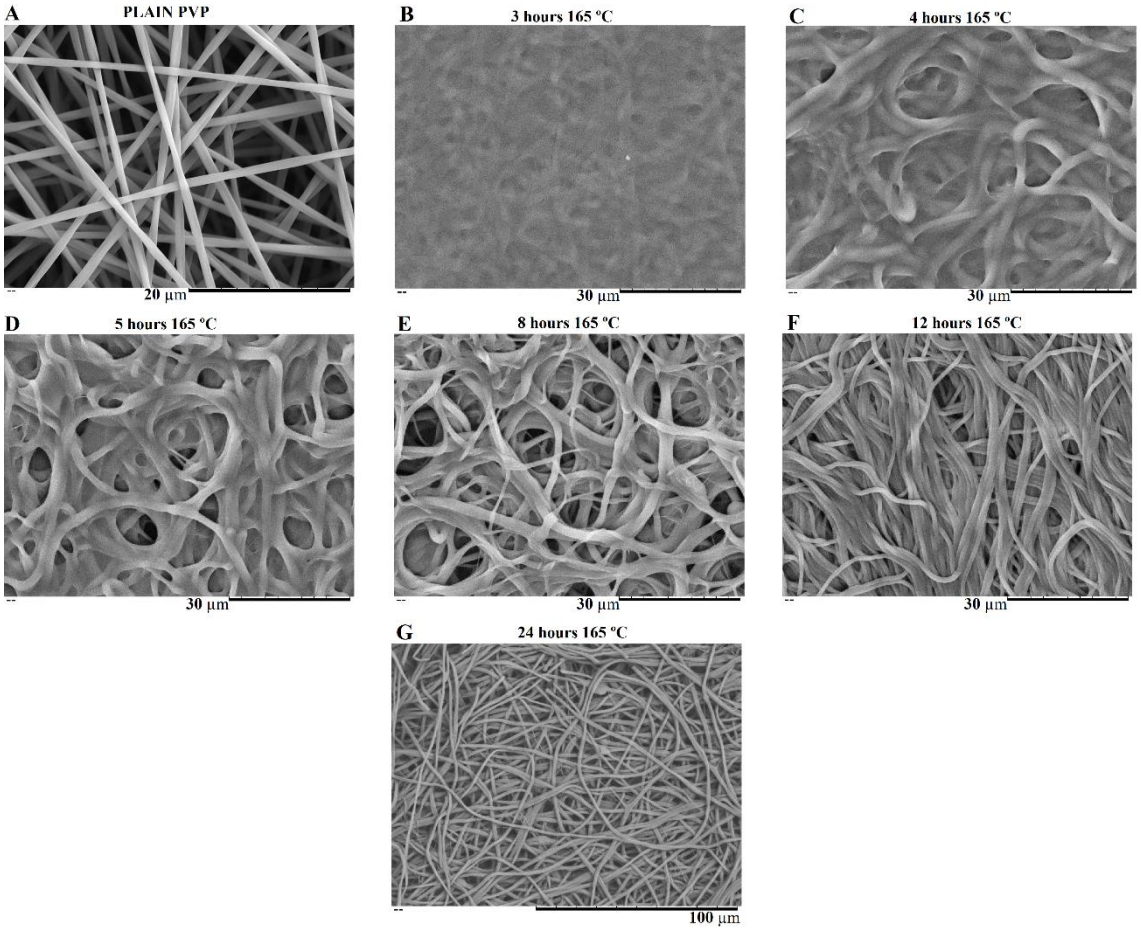

Fig. 6. SEM image of electrospun plain PVP before soaking into PBS (A), and SEM images of plain PVP thermal crosslinked at 165 °C for 3 h (B), 4 hours (C), 5 hours (D), 8 hours (E), 12 hours (F), and 24 hours (G) after soaking in PBS for 1 day.

SEM images of **Fig. 6** show the electrospun plain PVP before and after soaking in PBS for 24 hours, depending on previous crosslinking time. **Fig. 7** shows a similar study for PVP/MBG (1:1) composites, to compare how the MBG particles incorporation affects the thermal crosslinking. Both pure PVP and PVP/MBG (1:1) thermal crosslinked for 3 hours appear to lose the fibrous structure and form a kind of rough film without porosity. However, several differences were noticed: the fibrous structure of the plain PVP membranes crosslinked for 4 and 5 hours was not completely lost but appears as if the adjacent fibers have fused together and significantly reduced the porosity, whereas the composites crosslinked for 4 and 5 hours completely lose the fiber structure. In the case of the membranes crosslinked for 8 hours the fibrous structure of the membranes is still observed in both plain PVP and PVP/MBG (1:1), but the thickening of the fibers was clearly observed. In general, as the crosslinking time increases, the majority of the morphological features have been found to remain intact. The results also show that MBG nanoparticles incorporation into the PVP fibers also reduces the degree of composites crosslinking for same crosslinking time and temperature when compared to pure PVP. The MBG incorporation yielded more heterogeneous and thicker fibers, thus the effect of the temperature on PVP crosslinking can be slightly affected due to the filtering effect [22].

Preprints (www.preprints.org) | NOT PEER-REVIEWED | Posted: 19 April 2023 doi:10.20944/preprints202304.0595.v1

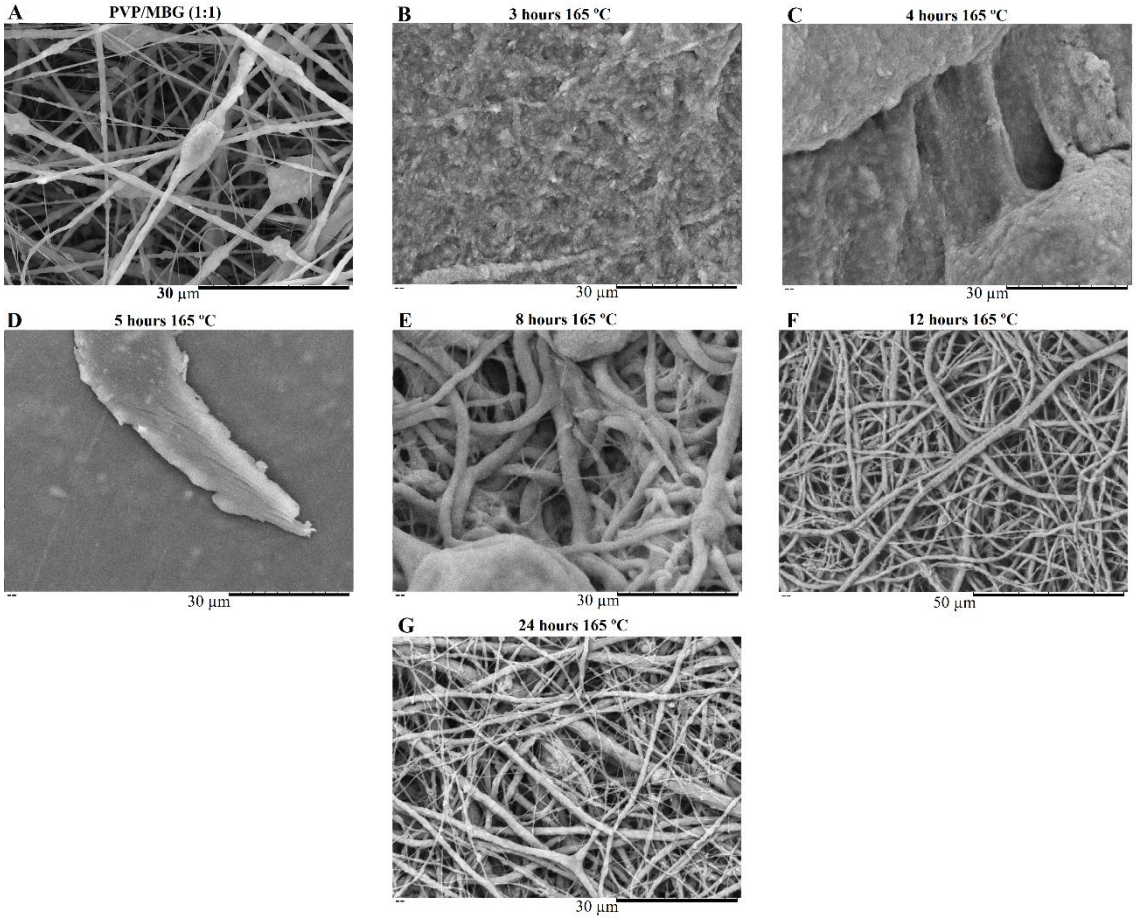

Fig. 7. SEM image of electrospun PVP/MBG (1:1) composite before soaking into PBS (A), and SEM images of PVP/MBG (1:1) composites thermal crosslinked at 165 °C for 3 h (B), 4 hours (C), 5 hours (D), 8 hours (E), 12 hours (F), and 24 hours (G) after soaking in PBS for 1 day.

3.3.2. Degradation Assay

The degradation rate of a scaffold is a key parameter for bone tissue engineering since it should match with the rate of neogenesis of ECM. The time required for bone healing varies according to the fracture configuration and location, status of the adjacent soft tissues, as well as patient characteristics (e.g. species, age, health status, and concurrent injuries/diseases). In general, bone healing time ranges from 6 weeks to 6 months [23–25]. Therefore, the *in vitro* biodegradation was studied by measuring the weight loss of the fiber mats in PBS at 37 °C for 4 weeks. **Fig. 8 A** represents the degradation ratio of PVP/MBG composites thermal crosslinked at 165 °C for 24 hours with different amount of MBG incorporated into the PVP fibers ranging from 10 to 100 % of polymer's mass. Pure PVP (also mentioned as plain PVP) was used as a control and revealed no mass loss during the assay, while the composite with a weight percentage of MBG equal to 100 % of PVP mass (also mentioned as PVP/MBG (1:1)) revealed a mass loss around 30 % after 28 days. Moreover, the data shows that scaffold mass loss increases with the MBG content for the same soaking time in PBS. This indicated that the inclusion of MBG particles accelerated the degradation rate of the fibrous mats. It was explained due to the high affinity of the MBG 80S15 with water, which increased the ability of the composites to absorb and retain water from the medium during the incubation periods and, consequently raised the hydrolytic degradation of PVP fibers [26]. On the other hand, the MBG dissolution over time also explains the increasing mass loss for composites with higher MBG contents.

Preprints (www.preprints.org) | NOT PEER-REVIEWED | Posted: 19 April 2023 doi:10.20944/preprints202304.0595.v1

Fig. 8 B and **C** represents the degradation assay for electrospun plain PVP membranes and PVP/MBG (1:1) composites, respectively. The samples were thermal crosslinked at 165°C for different times: 3, 4, 5, 8, 12, and 24 hours. Generally, polymer degradation kinetic is affected by their chemical and structural characteristics. In general, both graphics show that the degradation ratio decreases as the crosslinking time increase, except for the PVP/MBG (1:1) composites crosslinked for 8, 12, and 24 hours, which presented similar degradation ratios over time. This behavior was expected because the thermal crosslinking can enhance the thermal and chemical stabilities of PVP to form a stable network structure [27]. However, for the same thermal crosslinking conditions, the incorporation of MBG accentuate the degradation ratio compared to pure PVP. Furthermore, membranes with a low degree of crosslinking quickly lead to the high exposure of MBG particles to the medium. Consequently, the particles can be separated from PVP fibers, thus accelerating the degradation ratio even more. The degradation ratio data of PVP/MBG (1:1) thermal crosslinked for 3 hours is not shown in the graph because the samples partially lose their physical integrity. It is worth pointing out that all studied samples showed a fast degradation ratio in the first 2 hours, then the degradation was very slow or reached a plateau.

In general, the degradation ratios studied are in concordance with the overall structural changes for the samples after 24 hours of immersion in PBS (**Fig. 6** Fig**. 7**).

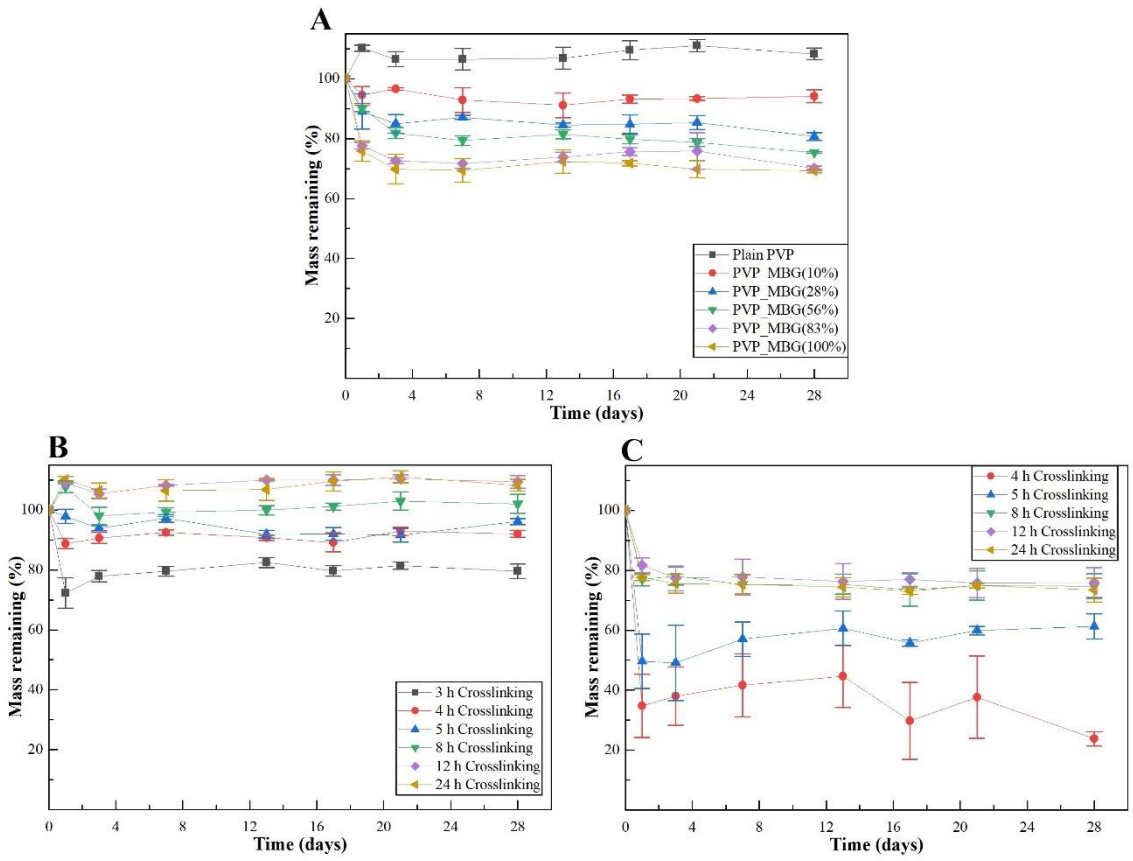

Fig. 8. Degradation assay for PVP/MBG composites (thermal crosslinked at 165 °C for 24 hours) with different MBG 80S15 content: 0, 10, 28, 56, 83, and 100 % of PVP mass (A); Degradation assay for electrospun PVP membranes (B) and PVP/MBG (1:1) composites (C) thermal crosslinked at 165 °C for different times: 3, 4, 5, 8, 12, and 24 hours.

3.3.3. Swelling Assay

Fig. 9 A and **B** show the swelling assay for different PVP/MBG composites depending on MBG content and thermal crosslinking duration, respectively. For each of the

Preprints (www.preprints.org) | NOT PEER-REVIEWED | Posted: 19 April 2023 doi:10.20944/preprints202304.0595.v1

membranes studied, the water absorption continues to increase until equilibrium is reached (approximately 24 hours of incubation). Plain PVP was used as control and its swelling ratio was calculated at around 500 %, whereas the data show as the amount of incorporated MBG increases, the swelling ratio also increases. The PVP/MBG (1:1) composite had the highest swelling ratio around 750–800 %. The hydrophilic character of PVP, the high surface area of the matrices, and the presence of MBG nanoparticles inside the fibers are factors that positively affect the swelling capability of the scaffolds since it is dependent on the degree of water uptake by pure polymer or composites. On the other hand, the PVP/MBG (1:1) composites crosslinked for 8, 12, and 24 hours showed different swelling capacities (**Fig. 9 B**). As discussed above, **Fig. 7 E**, **F**, and **G** illustrate the respective composites after 24 hours of immersion in PBS. It can be noticed that PVP fibers reduce the structural changes after being immersed in PBS as the crosslinking time increases, thus the water uptake from the medium and the capacity to retain such water reaches higher levels. Another study also reported the degree of swelling of polyester elastomers is an important parameter in characterizing their crosslinking degree [28]. Scaffolds with swelling capacity are highly desirable, particularly for drug delivery purposes where the drug can be trapped in the polymeric composite material and then released in a controlled manner.

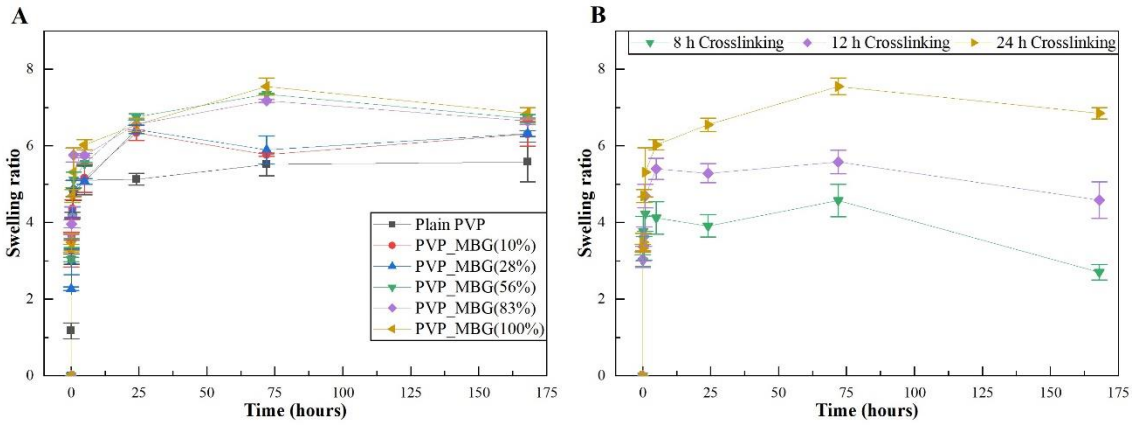

Fig. 9. Swelling assay for PVP/MBG composites (thermal crosslinked at 165 °C for 24 h) with different MBG 80S15 content: 0, 10, 28, 56, 83, and 100 % of PVP mass (A); Swelling assay for PVP/MBG (1:1) composites crosslinked for different times: 8, 12, and 24 hours (B).

3.4. Mechanical response – tensile tests

The different membranes of PVP and PVP/MBG (1:1) composites thermal crosslinked at 165 °C for 8, 12, and 24 hours were submitted to uniaxial stress-strain tests as shown in **These results** allow us to investigate the effect of thermal crosslinking and MBG nanoparticle incorporation on the mechanical properties of the electrospun matrices.

The comparison between plain PVP (**Fig. 10 A**) and PVP/MBG (1:1) (**Fig. 10 B**) stress-strain curves shows that mechanical properties were significantly modified with the MBG nanoparticles incorporation. With the incorporation of MBG nanoparticles, plastic deformation of the composite membranes is almost negligible since membrane rupture occurs almost immediately. This behaviour is characteristic of brittle materials. Furthermore, the three mechanical parameters that characterize the membranes were obtained from the stress-strain curves: Young's Modulus (E); the yield strength (σYS); and the ultimate tensile strength (UTS). The results for each membrane are shown in Table 2 and corroborate the changes in the mechanical properties. The presence of MBG in the PVP fibres implies a significant reduction in the three mechanical parameters calculated. The Young's modulus decreases by a factor of around 14 up to 21 times with the presence of MBG nanoparticles. This decrease along with the reduction in UTS values could be justified by the

Preprints (www.preprints.org) | NOT PEER-REVIEWED | Posted: 19 April 2023 doi:10.20944/preprints202304.0595.v1

increase in the inhomogeneity in the average fibre diameter, as reported in the SEM and TEM images of the composites. In fact, the poor dispersion of MBG nanoparticles at high concentrations leads to the formation of clusters, which decreases the homogeneity of PVP fibres. Higher amount of MBG is suitable for the preservation of scaffolds bioactivity, but it is likely to be responsible for the brittle mechanical behaviour of the composite samples. Reducing the amount of MBG particles inside the composite matrices leads to a trade-off between high mechanical properties and bioactivity. However, the high bioactivity of the composite fibres in necessary for BTE applications [29, 30]. In fact, other researchers have already reported that there is a threshold limit for bioactive glass particles concentration beyond which the nanoparticles caused a defective situation rather than reinforcing the polymer matrices, so that the nanocomposites became more brittle [26].

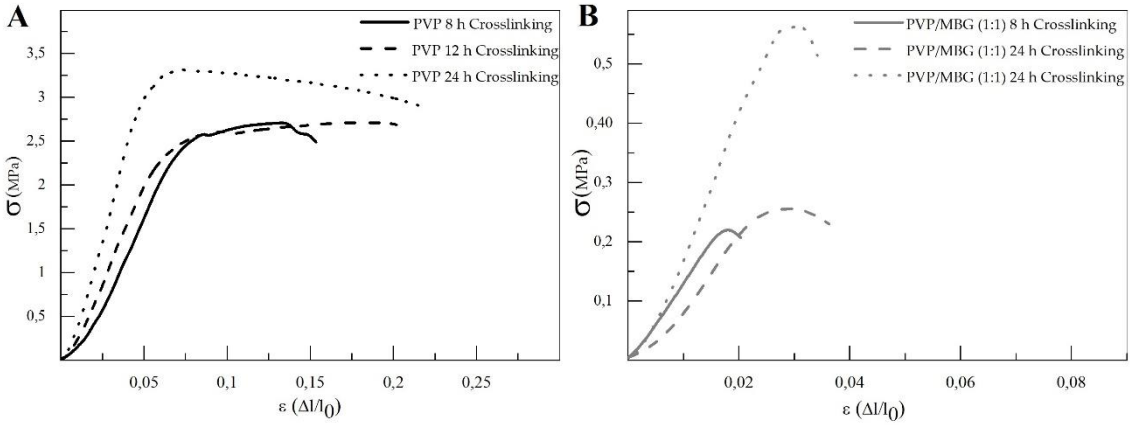

Fig. 10. These results allow us to investigate the effect of thermal crosslinking and MBG nanoparticle incorporation on the mechanical properties of the electrospun matrices.

The comparison between plain PVP (**Fig. 10 A**) and PVP/MBG (1:1) (**Fig. 10 B**) stress-strain curves shows that mechanical properties were significantly modified with the MBG nanoparticles incorporation. With the incorporation of MBG nanoparticles, plastic deformation of the composite membranes is almost negligible since membrane rupture occurs almost immediately. This behaviour is characteristic of brittle materials. Furthermore, the three mechanical parameters that characterize the membranes were obtained from the stress-strain curves: Young's Modulus (E); the yield strength (σ_{YS}); and the ultimate tensile strength (UTS). The results for each membrane are shown in Table 2 and corroborate the changes in the mechanical properties. The presence of MBG in the PVP fibres implies a significant reduction in the three mechanical parameters calculated. The Young's modulus decreases by a factor of around 14 up to 21 times with the presence of MBG nanoparticles. This decrease along with the reduction in UTS values could be justified by the increase in the inhomogeneity in the average fibre diameter, as reported in the SEM and TEM images of the composites. In fact, the poor dispersion of MBG nanoparticles at high concentrations leads to the formation of clusters, which decreases the homogeneity of PVP fibres. Higher amount of MBG is suitable for the preservation of scaffolds bioactivity, but it is likely to be responsible for the brittle mechanical behaviour of the composite samples. Reducing the amount of MBG particles inside the composite matrices leads to a trade-off between high mechanical properties and bioactivity. However, the high bioactivity of the composite fibres in necessary for BTE applications [29, 30]. In fact, other researchers have already reported that there is a threshold limit for bioactive glass particles concentration beyond which the nanoparticles caused a defective situation rather than reinforcing the polymer matrices, so that the nanocomposites became more brittle [26].

Preprints (www.preprints.org) | NOT PEER-REVIEWED | Posted: 19 April 2023 doi:10.20944/preprints202304.0595.v1

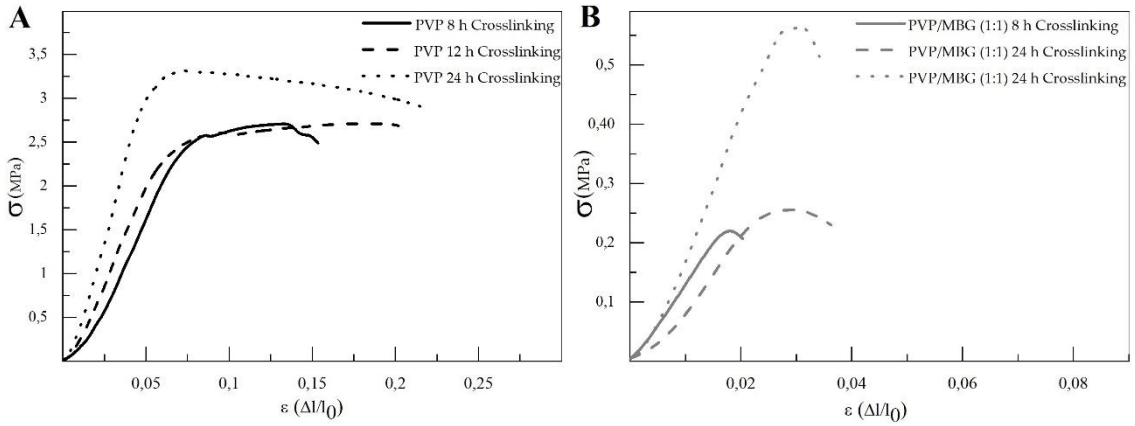

Fig. 10. Representative stress-strain curves of plain PVP and PVP/MBG (1:1) composite membranes crosslinked for different times: 8, 12, and 24 hours.

The time of thermal crosslinking also affected the mechanical properties of the samples. In general, the changes were very similar for plain PVP and PVP/MBG (1:1) composites. For instance, the plain PVP samples crosslinked for 8 and 12 hours exhibited a similar mechanical behaviour under tensile forces, which also occurred for PVP/MBG (1:1) composites crosslinked during 8 and 12 hours. Furthermore, when the samples were crosslinked for 24 hours, the mechanical parameters reached higher values. The Young's modulus increases by a factor of around 1.8 up to 1.9 when the crosslinking time increases from 8 to 24 hours, in both PVP and PVP/MBG (1:1) composites. In general, it is expected that crosslinking processes affect the mechanical properties of polymers since new interactions between polymer chains are being created. These results show that more crosslinking time is responsible for enhancing the mechanical strength of the samples. Thus, for periods of 8 and 12 hours at 165 °C, the crosslinking process is not complete yet, while 24 hours of thermal crosslinking mean higher bonding levels between the PVP chains.

Table 2. Calculated mechanical parameters for each membrane type: Young's modulus (E), ultimate tensile strength (UTS) and yield strength (σ_Y).

Sample	E (MPa)	UTS (MPa)	σ_Y (MPa)
PVP 8 h crosslinking	39.2 ± 10.9	2.45 ± 0.50	2.77 ± 056
PVP 12 h crosslinking	45.7 ± 14.1	2.27 ± 0.35	2.75 ± 0.44
PVP 24 h crosslinking	70.0 ± 16.2	3.01 ± 0.28	3.39 ± 0.38
PVP/MBG (1:1) 8 h crosslinking	11.9 ± 3.4	0.22 ± 0.07	0.23 ± 0.05
PVP/MBG (1:1) 12 h crosslinking	13.2 ± 2.5	0.23 ± 0.03	0.26 ± 0.05
PVP/MBG (1:1) 24 h crosslinking	22.9 ± 3.9	0.58 ± 0.09	0.59 ± 0.07

3.5. Cytotoxicity assays

Cytotoxicity assays were performed to evaluate the cytotoxic effect of produced MBG powder, electrospun PVP, and PVP/MBG (1:1) composites using the extract method. **Fig. 11** shows cell viability after incubation with 20 mg.mL^{-1} of each type of membrane studied, and the respective two-fold dilutions. In general, the results show an absence of cytotoxic effects for Saos-2 cells, except for plain PVP membrane previously thermal crosslinked at 165 °C for 8 hours, when the extract concentration tested was 20 mg.mL^{-1}. It may contrast with some researchers who have reported an increasing interest in PVP towards its use in biomedical applications due to its inertness, chemical stability, and biocompatibility [12]. However, to further understand these results, it is worth pointing out that the PVP was previously thermally crosslinked. At elevated temperatures, the stability of PVP decreases and leads to the opening of the pyrrolidone ring fractions. This phenomenon results in the transfer of hydrogen atoms from one radical to another, which leads to the formation of

Preprints (www.preprints.org) | NOT PEER-REVIEWED | Posted: 19 April 2023 doi:10.20944/preprints202304.0595.v1

double bonds by hydrogen donor and saturation of acceptor by the crosslinking process [31]. Furthermore, it can be found in the literature that the biocompatibility of PVP-based materials depends on the PVP content, and the changes in pyrrolidone rings, which may lead to the consequent loss of biocompatibility [32]. On the other hand, there are few reports about the thermal crosslinking process of PVP, and the effect of MBG nanoparticles incorporation on the thermal behavior of electrospun PVP fibers. However, the results presented here may lead to the hypothesis that electrospun PVP matrices were not fully crosslinked at 165 °C for 8 hours (in concordance with tensile tests), which may indicate the presence of open pyrrolidone rings, consequently decreasing its biocompatibility. However, after a two-fold dilution of the extract concentration to 10 mg.mL^{-1}, the cell viability rises near 100 %. This is in concordance with the cell viability of the PVP/MBG (1:1) composite crosslinked in the same conditions of the above-mentioned PVP membrane (165 °C for 8 h). The concentration of 20 mg.mL^{-1} for this composite means an individual concentration equal to 10 mg.mL^{-1} of both PVP and MBG 80S15. For this concentration both individual materials revealed no cytotoxic effects, thus the PVP/MBG (1:1) composite also revealed the absence of cytotoxicity.

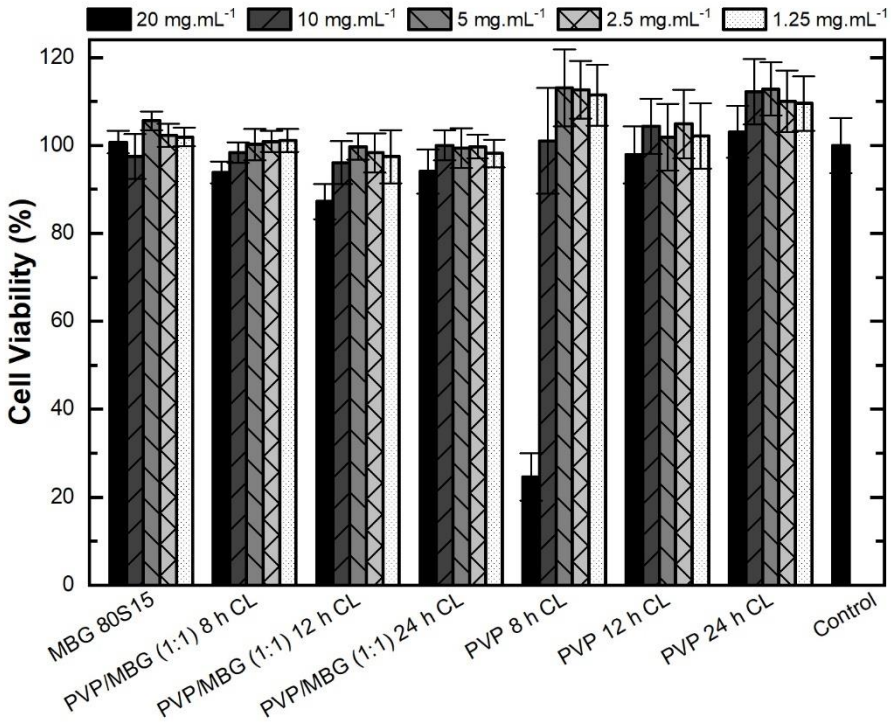

Fig. 11. Osteoblast cell line viability after 48 h exposure to diverse types of PVP membranes through indirect method (CL stands for crosslinking). Data is expressed as average ± standard deviation for at least five independent experiments.

3.6. Bioactivity assay

The bioactivity of MBG 80S15 pellets and PVP/MBG (1:1) composites was investigated in vitro by soaking the samples in SBF to detect the formation of HA on the surface. The samples were characterized by SEM, XRD, and FTIR.

Fig. 12 shows SEM images of MBG 80S15 before and after different immersion intervals in SBF. Before soaking in SBF solution (**Fig. 12 A**), the MBG particle's surface was smooth. After soaking for 24 h, the surfaces of the MBG pellets have important changes. It can be observed that a layer composed of needle-shaped crystallites fully covered the surface. EDS analysis confirmed that the chemical composition can be assigned to an HCA phase considering the Ca/P ratio slightly below 1.67 (Table 3). Furthermore, the thickness of the HCA layer continues to growth over time. After 5 days of immersion, cauliflower-

Preprints (www.preprints.org) | NOT PEER-REVIEWED | Posted: 19 April 2023 doi:10.20944/preprints202304.0595.v1

like clusters with needlelike crystallites shape spontaneously to reduce surface energy. These clusters grow over time, so that after MBG soaking in SBF for 10 days all the surface is covered with cauliflower-like clusters.

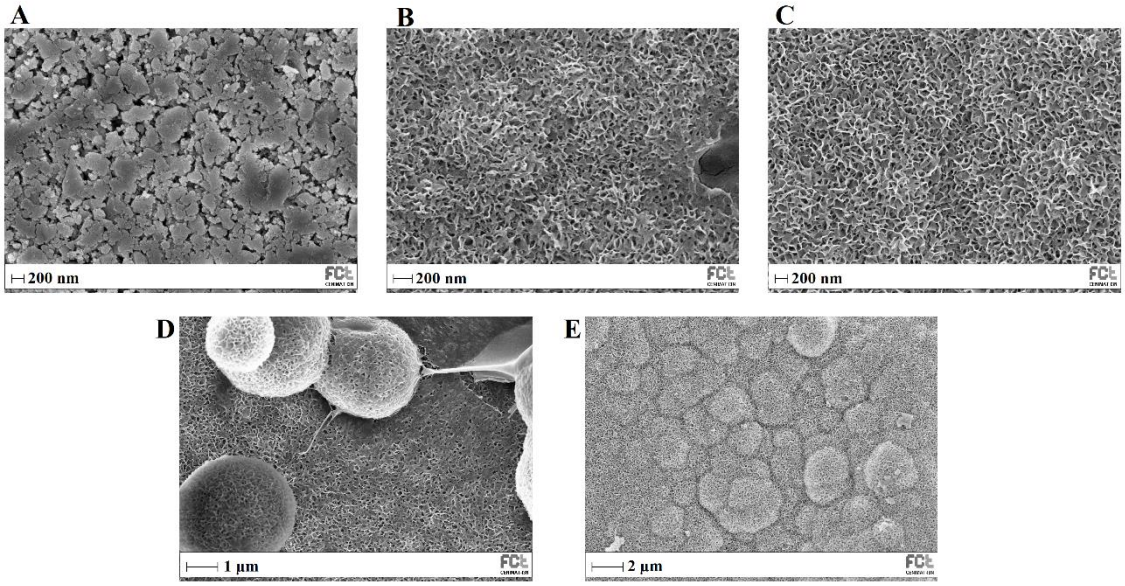

Fig. 12. SEM images of MBG 80S15 before (A) and after soaking in SBF for 1 day (B), 3 days (C), 5 days (D), and 10 days (E).

The respective XRD results of the MBG 80S15 pellets soaked in SBF for 1, 3, 5, and 10 days are shown in **Fig. 13 A**. As mentioned before, MBG showed the common broad band of amorphous materials at about 15-35°(2θ) before soaking in SBF. After 1 day of immersion in SBF, the XRD pattern of MBG 80S15 showed a major peak located at 32° (2θ) and another peak located at 26°(2θ), which could be assigned to the (211) and (002) reflection of an apatite-like phase [9]. After immersing for 3 days, the four new diffraction peaks at 39, 46, 49, and 53° (2θ) were assigned to the (310), (222), (213), and (004) reflections of HCA, respectively. As the immersion and mineralization time increased to 5 days, the diffraction peaks became more intense. The above-mentioned newly formed diffraction peaks are in accordance with the standard card of HCA (JCPD 24-0033). The XRD results demonstrated that the MBG 80S15 had good bioactivity in vitro and their mineralization product was HCA. Furthermore, the crystallinity of HCA became higher as immersion time increased [1].

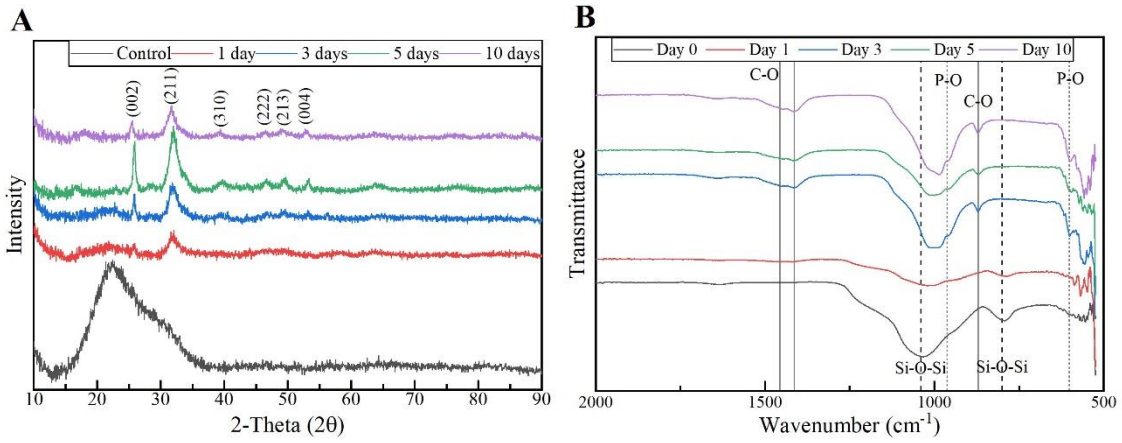

Fig. 13. XRD patterns (A) and FTIR spectra (B) of MBG 80S15 after soaking in SBF for different periods of time.

Preprints (www.preprints.org) | NOT PEER-REVIEWED | Posted: 19 April 2023 doi:10.20944/preprints202304.0595.v1

The growth of HCA on MBG 80S15 surface was further investigated by FTIR spectroscopy analysis. **Fig. 13 B** illustrates the IR spectra for MBG 80S15C samples after the same time periods soaked in SBF that were studied by SEM. Before immersion in SBF, the adsorption bands at 800 and 1040 cm^{-1} can be indexed to Si-O-Si bonds. However, when soaking in SBF for 3 days, three P–O crystalline vibrational bands near to 568, 602, and 963 cm^{-1} were detected (the noise near 500 cm^{-1} hindered the accurate analysis of 568 cm^{-1} band). Furthermore, other three new vibrational bands were detected near to 1456, 1414, and 870 cm^{-1}, which are assigned with C-O bond indicating the growth of the HCA layer on the surface of MBG 80S15 [33–35].

The above SEM, XRD, and FTIR results indicate that the MBGs 80S15 can induce the formation of an HCA layer on their surface even for short SBF soaking periods, which corroborates the superior in vitro bone forming bioactivity. Therefore, pointing out the interesting properties of the MBG 80S15 as a material for bone tissue engineering.

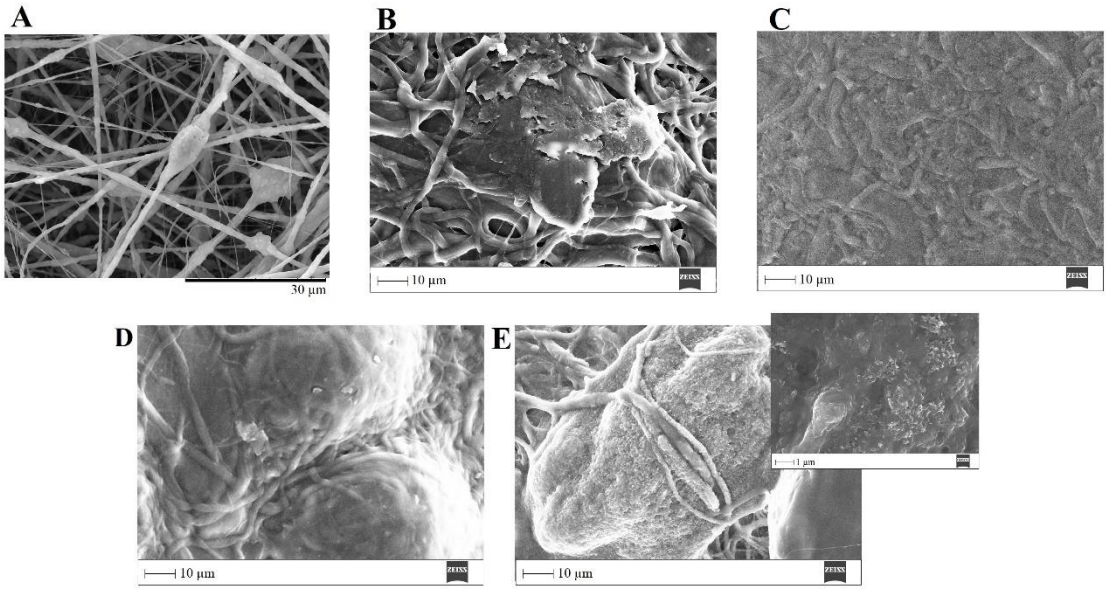

Fig. 14. SEM images of PVP/MBG (1:1) composite crosslinked for 8 h before (A) and after soaking in SBF for 1 day (B), 3 days (C), 5 days (D), and 10 days (E, and respective inset micrograph at higher magnification).

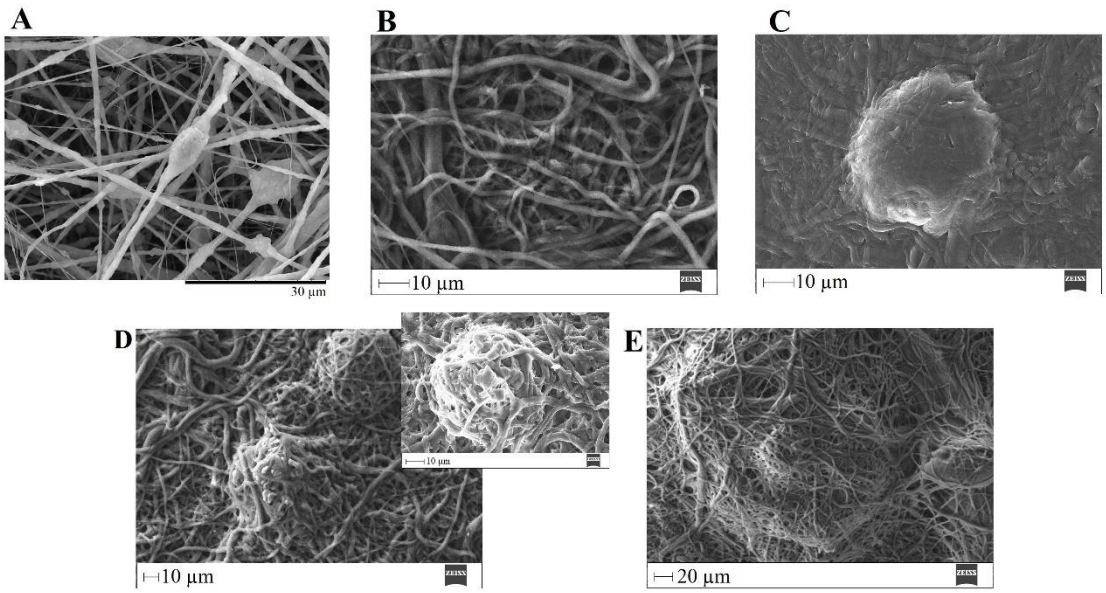

Preprints (www.preprints.org) | NOT PEER-REVIEWED | Posted: 19 April 2023 doi:10.20944/preprints202304.0595.v1

Fig. 15. SEM images of PVP/MBG (1:1) composite crosslinked for 12 h before (A) and after soaking in SBF for 1 day (B), 3 days (C), 5 days (D, and respective inset micrograph), and 10 days (E).

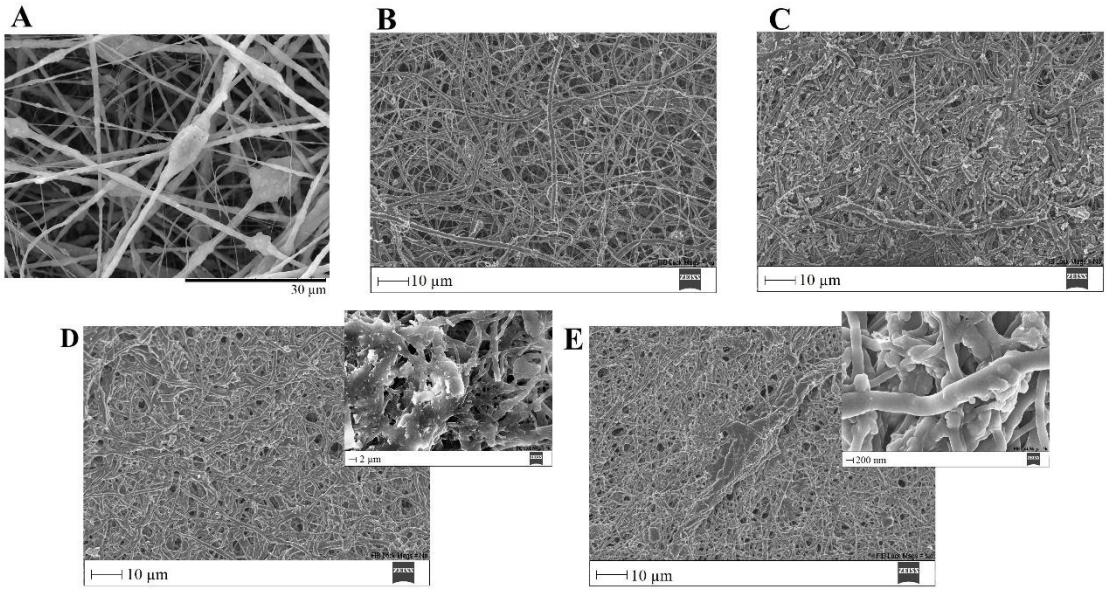

Fig. 16. SEM images of PVP/MBG (1:1) composite crosslinked for 24 h before (A) and after soaking in SBF for 1 day (B), 3 days (C), 5 days (D, and respective inset micrograph), and 10 days (E, and respective inset micrograph).

The bone-bonding potential of a biomaterial is often estimated by examining its ability to form the HCA layer on its surface when exposed to SBF. In order to study the formation of this layer, the PVP/MBG (1:1) composite scaffolds were also analysed by SEM, XRD, and FTIR before and after being soaked in SBF. Furthermore, the bioactive behaviour of the composite scaffolds is also dependent on the degradation ratio of the polymeric matrices, which in turn is dependent on the crosslinking conditions. To study the best crosslinking conditions considering the effect on enhancing the bioactivity of the scaffolds, the bioactivity assay was carried out on scaffolds crosslinked at 165 °C for 8 hours (**Fig. 14**), 12 hours (**Fig. 15**), and 24 hours (**Fig. 16**). The SEM analysis of the surface morphology of the scaffolds before and after soaking in SBF for 1, 3, 5 and 10 days. After immersion for 1 day, the surface of the samples crosslinked for 8, 12, and 24 hours becomes rougher. The samples' porosity decreases when compared with the samples before immersion in SBF, this effect is more accentuated for the samples crosslinked for 8 and 12 hours. Several precipitates were clearly observed on the nanocomposite surface over immersion time. However, this effect is delayed for samples crosslinked for 24 hours, probably due to the slower degradation of the PVP fibres hindering the contact between MBG glass particles and the medium. The bioactivity of the scaffolds can be clearly noticed for the samples crosslinked for 8 and 12 hours with the micrographs showing the spherical structures associated with the typical cauliflower-like structure. However, there are PVP fibres that have not been completely degraded yet. **Fig. 14 E** and the respective inset micrograph show that HCA growth stretches the PVP fibres, this phenomenon can accelerate the degradation rate of the scaffolds when compared with the degradation rate studied for immersion in PBS. It is worth pointing out that the above-mentioned makes it impossible to evaluate the bioactivity of composites crosslinked for 3, 4, and 5 hours since the samples did not keep their physical integrity when soaked into SBF.

EDS analysis (Table 3) of the nanofibrous mats surface before and after soaking in SBF allowed the determination of the atomic concentration of silicon, calcium, and phosphorus. In general, all samples showed a decrease in silicon concentration over time, and an increase in calcium and phosphorus concentrations. Moreover, the earliest apatite precipitate is usually "Ca deficient" exhibiting a Ca/P ratio below 1.67. Throughout the HCA

Preprints (www.preprints.org) | NOT PEER-REVIEWED | Posted: 19 April 2023 doi:10.20944/preprints202304.0595.v1

layer formation, the HA composition increases, and the Ca/P ratio also increases asymptotically towards Ca/P≈1.67 [36].

Table 3. Atomic concentration (At. %) of silicon (Si) and respective Ca/P ratio during the bioactivity assay for the different types of membrane studied and MBG 80S15 pellets before (control) and after soaking in SBF for 1, 3, 5, and 10 days. These results were obtained from EDS analysis (CL stands for crosslinking).

EDS (At. %)	Control		1 day		3 days		5 days		10 days	
Sample	Ca/P	Si	Ca/P	Si	Ca/P	Si	Ca/P	Si	Ca/P	Si
MBG 80S15 pellet	4.48	80.02	1.60	69.76	1.59	9.01	1.52	8.46	1.58	2.24
PVP/MBG (1:1) 8 h CL	1.49	73.59	1.48	89.89	0.75	85.96	1.23	34.48	1.64	0.60
PVP/MBG (1:1) 12 h CL	1.49	73.59	1.05	92.32	1.13	36.11	1.58	31.73	1.83	5.75
PVP/MBG (1:1) 24 h CL	1.49	73.59	1.43	85.69	1.47	77.99	3.72	85.66	1.22	66.24

In general, the SEM analysis for bioactivity assay of PVP/MBG (1:1) composites revealed quite similar results considering the HCA precipitation for samples crosslinked for 8 and 12 hours, while the HCA precipitation on fibres' surface seems to be delayed for the samples crosslinked for 24 hours.

To confirm the formation of the HCA layer on fibre's surface, the PVP/MBG (1:1) composites thermal crosslinked for 8, 12, and 24 hours were also analysed by XRD and FTIR before and after being soaked in SBF. XRD patterns are illustrated in Fig. 17 A, C, and E for the three types of scaffolds previously studied by SEM (8, 12, and 24 hours of thermal crosslinking). All samples exhibited no diffraction peaks before soaking in SBF, as expected due to the amorphous structure of both MBG and the PVP. However, significant changes in the XRD patterns occur after immersion in SBF for the three types of composite membranes. The samples thermal crosslinked for 8 hours revealed different diffraction peaks as the immersion time increased at 2θ = 26°, 32°, 40°, 46°, 49°, 53°, and 57°, which correspond to the reflection of crystalline planes with the Miller indices (002), (211), (310), (222), (213), (004), and (322), respectively. In the case of composites thermal crosslinked for 12 hours, as the SBF immersion time increased, the XRD patterns show diffraction peaks at 2θ = 32°, 46°, 53°, and 57°, which correspond to the reflection of crystalline planes with the Miller indices (211), (222), (004), and (322), respectively. Lastly, in the above-mentioned conditions, the XRD patterns of the composites thermal crosslinked for 24 hours show diffraction peaks at 2θ = 26°, 32°, 46°, and 57°, which correspond to the reflection of crystalline planes with the Miller indices (002), (211), (222), and (322), respectively. As previously discussed for MBG 80S15 bioactivity assay, the newly formed diffraction peaks for the three types of polymeric composites studied are in concordance with the standard card of HCA (JCPD 24-0033). The XRD patterns of the scaffolds thermal crosslinked for 8 and 12 hours showed sharper and more intense peaks when compared to the scaffolds thermal crosslinked for 24 hours. These results indicate higher crystallinity and large amounts of HCA present in the samples.

Preprints (www.preprints.org) | NOT PEER-REVIEWED | Posted: 19 April 2023 doi:10.20944/preprints202304.0595.v1

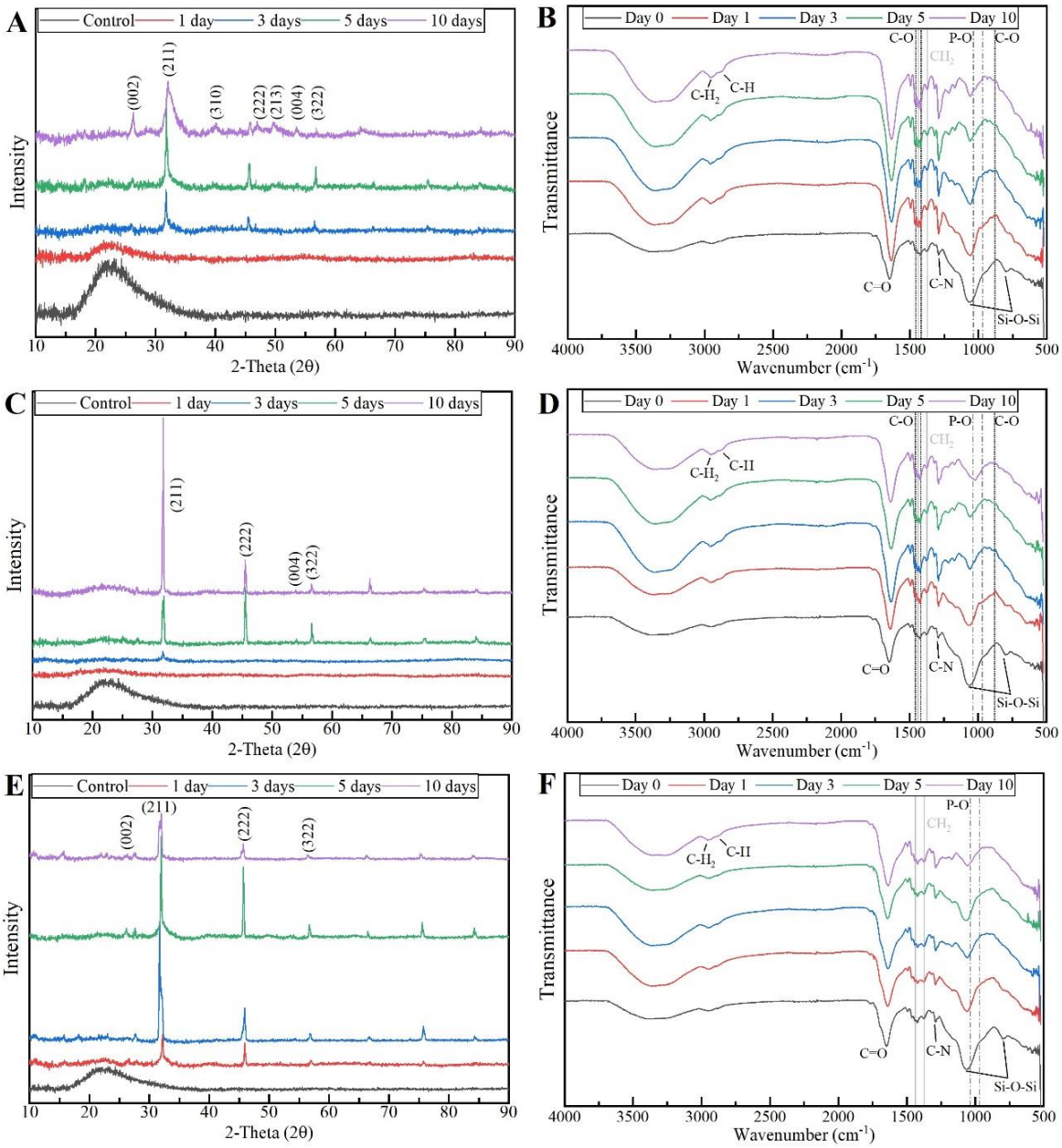

Fig. 17. XRD patterns and FTIR spectra of PVP/MBG (1:1) composites crosslinked for 8 h (A, B), 12 h (C, D), and 24 h (E, F) after soaking in SBF for different periods of time: 1, 3, 5, and 10 days.

These XRD results are in accordance with FTIR analysis, revealing the formation of the HCA structure. Starting with the FTIR spectrum of PVP/MBG (1:1) before immersion in SBF, the following absorption bands are assigned to the PVP: the band located around 1648 cm^{-1} can be ascribed to the stretching vibration of the C=O in the pyrrolidone group; the broad near to 2850-3000 cm^{-1} is associated with the CH stretching modes, which can be assigned to five overlapping signals: asymmetric CH_2 stretching (polymer chain: 2983 cm^{-1}, ring: 2954 cm^{-1}), symmetric CH_2 stretching (polymer chain: 2919 cm^{-1}; ring: 2885 cm^{-1}) and ternary CH (2852 cm^{-1}); the bands at 1427 cm^{-1} and 1372 cm^{-1} also correspond to the CH deformation modes from the CH_2 group; the absorption bands at 1288 cm^{-1} are related to C–N bending vibration from the pyrrolidone structure [37]. On the other hand, the adsorption bands at 470 (not shown in graphs due to the noise), 802, and 1058 cm^{-1} can be assigned to Si-O-Si bonds of the MBG 80S15. After immersion in SBF, the membranes thermal crosslinked for 8 and 12 hours showed similar FTIR spectra over time: the P–O

Preprints (www.preprints.org) | NOT PEER-REVIEWED | Posted: 19 April 2023 doi:10.20944/preprints202304.0595.v1

symmetric stretching vibrational bands near 970 cm^{-1} was detected (the noise near 500 cm^{-1} hindered the accurate analysis of the other two characteristics bands of the P–O bond: 568 and 600 cm^{-1}, associated with bending modes); after 5 days of immersion in SBF, the vibrational band near 970 cm^{-1} was no longer detected due to the shift of the 1058 cm^{-1} band assigned to Si-O-Si band. This shift was related to the overlapping of a new band at 1036 cm^{-1}, which is associated with the asymmetric stretching of P–O bond [38]; three vibrational bands near 1458, 1417, and 880 cm^{-1} were also detected and assigned with C-O bond. However, it was noticed the bands near to 1458 and 1417 cm^{-1} increased the intensity over immersion time, while the band at 880 cm^{-1} only reveal a slight change in intensity.

The above-mentioned changes in the FTIR spectra were not detected for the samples thermal crosslinked for 24 hours, except the shift associated with the new band at 1036 cm^{-1} after 10 days after immersion in SBF. The FTIR analysis are in accordance with the SEM results, indicating the growth of the HCA layer over time, which seem to be delayed for the scaffolds thermal crosslinked for 24 hours.

The mechanism of apatite formation upon contact of MBG 80S15 with SBF consists of five stages: 1) fast ion exchange of alkali ions with hydrogen ions from the liquid medium; 2) glass network dissolution; 3) silica-gel polymerization; 4) and 5) chemisorption and crystallization of the carbonated hydroxyapatite layer. The detailed analysis of the reactions involved has been reported by Hench [39]. Stages 1) and 2) explain the fading of the band at 802 cm^{-1} (Si-O-Si), which was noticed for all the scaffolds studied. Furthermore, stages 1 and 2 strongly depend on the PVP degradation rate, thus allowing us to state that crosslinking directly affects the bioactivity of the polymeric composite scaffolds studied. On the other hand, as shown in the swelling assay, the high wettability of PVP may favour the SBF interaction with the MBG nanoparticles, allowing the apatite mineralization inside PVP fibres and subsequent growth in the radial direction [40].

This study is consistent with the previous reports, which demonstrated that the inclusion of the BG particles into the polymeric matrices enhanced the in vitro hydroxyapatite formation onto the surface of the nanocomposites under a SBF medium. For instance, Lin et al,.[41], Allo *et al.*, [42], and Liverani *et al.*, [29] made different studies and achieve similar conclusions. The researchers found that the incorporation of bioactive glasses into a PCL [41, 42] and PCL/chitosan [29] nanofibrous matrices significantly enhanced its apatite formation ability in SBF compared with individual polymeric membranes. In addition, Han *et al.*, [43] indicated the higher bioactivity of composite nanofibers compared to pure PAN-based carbon nanofibers. Meanwhile, Yang *et al.*, [44] also reported that the presence of BG nanoparticles in the carbon nanofiber composites had increased the rates of the heterogeneous apatite nucleation [40].

4. Discussion

We report here the synthesis and characterization of MBG 80S15, which was successfully incorporated into the PVP fibrous mats by means of electrospinning process. In general, all PVP/MBG (1:1) composites crosslinked for 8, 12, and 24 h showed HCA forming ability. However, the impact of thermal crosslinking period on scaffolds' bioactivity should be considered as previously discussed. When the scaffolds were thermally crosslinked at 165 °C for 8 and 12 h, the bioactivity revealed similar results whereas the scaffolds crosslinked for 24 h showed a slower reactivity. These polymeric scaffolds also revealed the absence of cytotoxic effects on Saos-2 cells as intended for BTE applications. Moreover, the degradation ratio and swelling capacity of the produced composites can be tailored by varying the amount of MBG powder incorporated or the crosslinking conditions. The overall results indicated that the described electrospun nanocomposite fiber mats are promising bone scaffolds as they combine the high bioactivity of MBG 80S15 nanosized powder, and benefit from the flexibility of electrospun PVP mats. The main hurdle to face is to combine bioactivity and mechanical strength since the results showed a trade-off between bioactivity and mechanical strength for PVP/MBG (1:1) scaffolds. This

Preprints (www.preprints.org) | NOT PEER-REVIEWED | Posted: 19 April 2023 doi:10.20944/preprints202304.0595.v1

effect resulted from the inhomogeneity of PVP nanofibers' diameter with the incorporation of large amounts of MBG powder, which tends to agglomerate and form clusters.

5. Conclusions

Considering the presented results, the scaffolds thermally crosslinked for 12 h showed the most promising results. These scaffolds showed fast HCA layer formation, which was comparable to that obtained for scaffolds thermally crosslinked for 8 h. However, the composites crosslinked for 12 h are easier to handle, e.g., they keep their physical properties for longer periods when immersed in SBF solution. They also revealed high biocompatibility and suitable swelling capacity for further drug delivery applications combined with BTE.

Author Contributions: Conceptualization, R.M, P.S. and J.P.B.; methodology, R.M.; validation, P.S. and J.P.B.; formal analysis, R.M.; investigation, R.M.; writing—original draft preparation, R.M.; writing—review and editing, P.S., J.P.B., and J.C.S.; supervision, P.S., J.P.B., and J.C.S.; funding acquisition, P.S., J.P.B., and J.C.S. All authors have read and agreed to the published version of the manuscript.

Funding: This work is co-financed by FEDER, European funds, through the COMPETE 2020 POCI and PORL, National Funds through FCT—Portuguese Foundation for Science and Technology and POR Lisboa2020, under the project POCI-01-0145-FEDER- 007688, reference UIDB/50025/2020-2023, and project DREaMM, reference PTDC/CTM-CTM/30623/2017. The authors also acknowledge the support of FCT, in the scope of the projects LA/P/0037/2020, UIDB/50025/2020 and UIDP/50025/2020 of the Associate Laboratory Institute of Nanostructures, Nanomodelling and Nanofabrication-i3N. Ricardo Matos acknowledges FCT for the PhD grant with reference SFRH/BD/140090/2018.

Institutional Review Board Statement: Not applicable.

Data Availability Statement: The data presented in this study are available on request from the corresponding author.

Conflicts of Interest: The authors declare no conflict of interest.

References

1. J. Chen, L. Zeng, X. Chen, T. Liao, and J. Zheng, "Preparation and characterization of bioactive glass tablets and evaluation of bioactivity and cytotoxicity in vitro," *Bioact Mater*, vol. 1, no. 7, Sep. 2017, doi: 10.1016/j.bioactmat.2017.11.004.
2. A. A. El-Rashidy, J. A. Roether, L. Harhaus, U. Kneser, and A. R. Boccaccini, "Regenerating bone with bioactive glass scaffolds: A review of in vivo studies in bone defect models," *Acta Biomaterialia*, vol. 62. Acta Materialia Inc, pp. 1–28, Oct. 15, 2017. doi: 10.1016/j.actbio.2017.08.030.
3. A. R. Amini, C. T. Laurencin, and S. P. Nukavarapu, "Bone Tissue Engineering: Recent Advances and Challenges," *Crit Rev Biomed Eng.*, vol. 40, no. 5, pp. 363–408, 2012.
4. Q. Z. Chen, I. D. Thompson, and A. R. Boccaccini, "45S5 Bioglass®-derived glass-ceramic scaffolds for bone tissue engineering," *Biomaterials*, vol. 27, no. 11, pp. 2414–2425, Apr. 2006, doi: 10.1016/j.biomaterials.2005.11.025.
5. A. A. Gorustovich, J. A. Roether, and A. R. Boccaccini, "Effect of Bioactive Glasses on Angiogenesis: A Review of In Vitro and In Vivo Evidences."
6. L. L. Hench and J. M. Polak, "Third-Generation Biomedical Materials," *Bodybuilding: The Bionic Human*, vol. 295, Feb. 2002.
7. A. R. Boccaccini, M. Erol, W. J. Stark, D. Mohn, Z. Hong, and J. F. Mano, "Polymer/bioactive glass nanocomposites for biomedical applications: A review," *Compos Sci Technol*, vol. 70, no. 13, pp. 1764–1776, Nov. 2010, doi: 10.1016/j.compscitech.2010.06.002.
8. L. L. Hench, R. J. Splinter, W. C. Allen, and T. K. Greenlee, "Bonding Mechanisms at the Interface of Ceramic Prosthetic Materials."
9. Y. Cao, L. Zhang, Y. Xu, X. Wang, and B. Liu, "Preparation and bioactivity of mesoporous bioactive glasses with different phosphorus contents," in *Advanced Materials Research*, 2011, pp. 1997–2002. doi: 10.4028/www.scientific.net/AMR.287-290.1997.
10. H. W. Kim, H. H. Lee, and G. S. Chun, "Bioactivity and osteoblast responses of novel biomedical nanocomposites of bioactive glass nanofiber filled poly(lactic acid)," *J Biomed Mater Res A*, vol. 85, no. 3, pp. 651–663, Jun. 2008, doi: 10.1002/jbm.a.31339.

Preprints (www.preprints.org) | NOT PEER-REVIEWED | Posted: 19 April 2023 doi:10.20944/preprints202304.0595.v1

11. E. Palin, H. Liu, and T. J. Webster, "Mimicking the nanofeatures of bone increases bone-forming cell adhesion and proliferation," *Nanotechnology*, vol. 16, no. 9. pp. 1828–1835, Sep. 01, 2005. doi: 10.1088/0957-4484/16/9/069.
12. M. Kurakula and G. S. N. Koteswara Rao, "Moving polyvinyl pyrrolidone electrospun nanofibers and bioprinted scaffolds toward multidisciplinary biomedical applications," *European Polymer Journal*, vol. 136. Elsevier Ltd, Aug. 05, 2020. doi: 10.1016/j.eurpolymj.2020.109919.
13. X. Yan, C. Yu, X. Zhou, J. Tang, and D. Zhao, "Highly ordered mesoporous bioactive glasses with superior in vitro bone-forming bioactivities," *Angewandte Chemie - International Edition*, vol. 43, no. 44, pp. 5980–5984, Nov. 2004, doi: 10.1002/anie.200460598.
14. T. E. Newsome and S. V. Olesik, "Electrospinning silica/polyvinylpyrrolidone composite nanofibers," *J Appl Polym Sci*, vol. 131, no. 21, Nov. 2014, doi: 10.1002/app.40966.
15. T. Kokubo and H. Takadama, "How useful is SBF in predicting in vivo bone bioactivity?," *Biomaterials*, vol. 27, no. 15, pp. 2907–2915, 2006, doi: 10.1016/j.biomaterials.2006.01.017.
16. T. Kokubo, H. Kushitani, S. Sakka, T. Kitsugi, and T. Yamamum, "Solutions able to reproduce in vivo surface-structure changes in bioactive glass-ceramic A-W3."
17. "ISO/FDIS 23317 Implants for surgery-In vitro evaluation for apatite-forming ability of implant materials Implants chirurgicaux-Évaluation in vitro de la capacité de formation d'apatite des matériaux d'implants," 2007. [Online]. Available: www.iso.org
18. X. X. Yan *et al.*, "Mesoporous bioactive glasses. I. Synthesis and structural characterization," *J Non Cryst Solids*, vol. 351, no. 40–42, pp. 3209–3217, Oct. 2005, doi: 10.1016/j.jnoncrysol.2005.08.024.
19. J. Yi, G. Wei, X. Huang, L. Zhao, Q. Zhang, and C. Yu, "Sol-gel derived mesoporous bioactive glass fibers as tissue-engineering scaffolds," *J Solgel Sci Technol*, vol. 45, no. 1, pp. 115–119, Jan. 2008, doi: 10.1007/s10971-007-1668-x.
20. G. M. Luz and J. F. Mano, "Preparation and characterization of bioactive glass nanoparticles prepared by sol-gel for biomedical applications," *Nanotechnology*, vol. 22, no. 49, Dec. 2011, doi: 10.1088/0957-4484/22/49/494014.
21. K. M. Hatch, J. Hlavatá, K. Paulett, T. Liavitskaya, S. Vyazovkin, and A. V. Stanishevsky, "Nanocrystalline cellulose/polyvinylpyrrolidone fibrous composites prepared by electrospinning and thermal crosslinking," *Int J Polym Sci*, vol. 2019, 2019, doi: 10.1155/2019/7103936.
22. R. Fogaça and L. H. Catalani, "PVP hydrogel membranes produced by electrospinning for protein release devices," *Soft Mater*, vol. 11, no. 1, pp. 61–68, 2013, doi: 10.1080/1539445X.2011.580411.
23. K. Kumar, R. S. Gill, and U. Batra, "Challenges and opportunities for biodegradable magnesium alloy implants," *Materials Technology*, vol. 33, no. 2. Taylor and Francis Ltd., pp. 153–172, Jan. 28, 2018. doi: 10.1080/10667857.2017.1377973.
24. D. Bellucci, A. Sola, and V. Cannillo, "Hydroxyapatite and tricalcium phosphate composites with bioactive glass as second phase: State of the art and current applications," *Journal of Biomedical Materials Research - Part A*, vol. 104, no. 4. John Wiley and Sons Inc., pp. 1030–1056, Apr. 01, 2016. doi: 10.1002/jbm.a.35619.
25. A. Bigham-Sadegh and A. Oryan, "Basic concepts regarding fracture healing and the current options and future directions in managing bone fractures," *International Wound Journal*, vol. 12, no. 3. Blackwell Publishing Ltd, pp. 238–247, Jun. 01, 2015. doi: 10.1111/iwj.12231.
26. M. Kouhi, M. Morshed, J. Varshosaz, and M. H. Fathi, "Poly (ε-caprolactone) incorporated bioactive glass nanoparticles and simvastatin nanocomposite nanofibers: Preparation, characterization and in vitro drug release for bone regeneration applications," *Chemical Engineering Journal*, vol. 228, pp. 1057–1065, Jul. 2013, doi: 10.1016/j.cej.2013.05.091.
27. X. Jin *et al.*, "Effects of thermal cross-linking on the structure and property of asymmetric membrane prepared from the polyacrylonitrile," *Polymers (Basel)*, vol. 10, no. 5, May 2018, doi: 10.3390/polym10050539.
28. R. Indira, T. Tamizharuvi, T. V Rajendran, and V. Jaisankar, "Synthesis and Characterisation of Certain Novel Polyester Elastomers," *Indian Journal of Advances in Chemical Science*, vol. 1, no. 4, pp. 250–255, Jul. 2013, [Online]. Available: www.ijacskros.com
29. L. Liverani *et al.*, "Incorporation of bioactive glass nanoparticles in electrospun PCL/chitosan fibers by using benign solvents," *Bioact Mater*, vol. 3, no. 1, pp. 55–63, Mar. 2018, doi: 10.1016/j.bioactmat.2017.05.003.
30. F. Serio, M. Miola, E. Vernè, D. Pisignano, A. R. Boccaccini, and L. Liverani, "Electrospun filaments embedding bioactive glass particles with ion release and enhanced mineralization," *Nanomaterials*, vol. 9, no. 2, Feb. 2019, doi: 10.3390/nano9020182.
31. V. Milosavljevic *et al.*, "Alternative Synthesis Route of Biocompatible Polyvinylpyrrolidone Nanoparticles and Their Effect on Pathogenic Microorganisms," *Mol Pharm*, vol. 14, no. 1, pp. 221–233, Jan. 2017, doi: 10.1021/acs.molpharmaceut.6b00807.
32. X. Liu, Y. Xu, Z. Wu, and H. Chen, "Poly(N-vinylpyrrolidone)-Modified surfaces for biomedical applications," *Macromolecular Bioscience*, vol. 13, no. 2. pp. 147–154, Feb. 2013. doi: 10.1002/mabi.201200269.
33. Z. Wu *et al.*, "Synthesis and characterization of mesoporous bioactive glasses with highly ordered structures and high surface areas by a self-assembly process," *J Non Cryst Solids*, vol. 517, pp. 1–8, Aug. 2019, doi: 10.1016/j.jnoncrysol.2019.05.007.

Preprints (www.preprints.org) | NOT PEER-REVIEWED | Posted: 19 April 2023 doi:10.20944/preprints202304.0595.v1

34. Y. Zhu *et al.*, "Preparation, characterization and in vitro bioactivity of mesoporous bioactive glasses (MBGs) scaffolds for bone tissue engineering," *Microporous and Mesoporous Materials*, vol. 112, no. 1–3, pp. 494–503, Jul. 2008, doi: 10.1016/j.micromeso.2007.10.029.
35. X. Yan *et al.*, "The in-vitro bioactivity of mesoporous bioactive glasses," *Biomaterials*, vol. 27, no. 18, pp. 3396–3403, Jun. 2006, doi: 10.1016/j.biomaterials.2006.01.043.
36. M. Edén, "Structure and formation of amorphous calcium phosphate and its role as surface layer of nanocrystalline apatite: Implications for bone mineralization," *Materialia (Oxf)*, vol. 17, Jun. 2021, doi: 10.1016/j.mtla.2021.101107.
37. I. A. Safo, M. Werheid, C. Dosche, and M. Oezaslan, "The role of polyvinylpyrrolidone (PVP) as a capping and structure-directing agent in the formation of Pt nanocubes," *Nanoscale Adv*, vol. 1, no. 8, pp. 3095–3106, 2019, doi: 10.1039/c9na00186g.
38. G. Zahra *et al.*, "Nanosized calcium-deficient carbonated hydroxyapatite synthesized by microwave activation," *J. Mater. Environ. Sci. 6 (4)*, pp. 983–988, 2015, [Online]. Available: https://www.researchgate.net/publication/281800019
39. L. L. Hench, "Bioceramics: From Concept to Clinic," *J. Am. Ceram. Soc., 74 [7]*, pp. 1487–510, 1991.
40. S. Ö. Gönen, M. Erol Taygun, and S. Küçükbayrak, "Fabrication of bioactive glass containing nanocomposite fiber mats for bone tissue engineering applications," *Compos Struct*, vol. 138, pp. 96–106, Mar. 2016, doi: 10.1016/j.compstruct.2015.11.033.
41. H. M. Lin, Y. H. Lin, and F. Y. Hsu, "Preparation and characterization of mesoporous bioactive glass/ polycaprolactone nanofibrous matrix for bone tissues engineering," *J Mater Sci Mater Med*, vol. 23, no. 11, pp. 2619–2630, Nov. 2012, doi: 10.1007/s10856-012-4734-z.
42. B. A. Allo, S. Lin, K. Mequanint, and A. S. Rizkalla, "Role of bioactive 3D hybrid fibrous scaffolds on mechanical behavior and spatiotemporal osteoblast gene expression," *ACS Appl Mater Interfaces*, vol. 5, no. 15, pp. 7574–7583, Aug. 2013, doi: 10.1021/am401861w.
43. B. Han *et al.*, "Improved bioactivity of PAN-based carbon nanofibers decorated with bioglass nanoparticles," *J Biomater Sci Polym Ed*, vol. 25, no. 4, pp. 341–353, Mar. 2014, doi: 10.1080/09205063.2013.861169.
44. Q. Yang *et al.*, "Osteocompatibility characterization of polyacrylonitrile carbon nanofibers containing bioactive glass nanoparticles," *Carbon N Y*, vol. 56, pp. 288–295, May 2013, doi: 10.1016/j.carbon.2013.01.014.